TAMPEREEN TEKNILLINEN YLIOPISTO
TAMPERE UNIVERSITY OF TECHNOLOGY

Jarno Riistama

Characterisation of Wearable and Implantable Physiological Measurement Devices

Julkaisu 879 • Publication 879

Tampere 2010

Tampereen teknillinen yliopisto. Julkaisu 879
Tampere University of Technology. Publication 879

Jarno Riistama

Characterisation of Wearable and Implantable Physiological Measurement Devices

Thesis for the degree of Doctor of Technology to be presented with due permission for public examination and criticism in Tietotalo Building, Auditorium TB111, at Tampere University of Technology, on the 7th of May 2010, at 12 noon.

Tampereen teknillinen yliopisto - Tampere University of Technology
Tampere 2010

ISBN 978-952-15-2347-2 (printed)
ISBN 978-952-15-2389-2 (PDF)
ISSN 1459-2045

ABSTRACT

Electrodes are an important part of any biopotential measurement application. The electrodes will be in direct galvanic contact with the skin or tissue of the measurement subject. The interface between the electrode and electrolyte has a complicated structure involving both physical and chemical processes and reactions. The thesis revises the complex interface in terms of reactions occurring at the interface, the formation and structure of the double layer at the interface, electrode potential, and various electrical equivalent interface models. The artefacts occurring at the interface are also introduced and possibilities to reduce them are discussed.

A relation between the artefacts and electrode materials is established through electrochemical noise measurements performed with several metallic electrodes as well as with textile electrodes. The electrochemical noise arising from the interface as a function of time reflects the stabilisation time of the current electrode–electrolyte interface. The electrochemical noise will reduce as time from the application of the electrode on the subject elapses. The time the interface needs to reach its steady state is called the stabilisation time of the electrode. Electrode materials that possess a short stabilisation time are the most suitable ones for applications where artefacts are probable. Such applications are the ones that involve e.g. motion or deformation of the skin of the subject.

Noise measurements were conducted with gold (Au), silver (Ag), silver–silver-chloride (Ag/AgCl), platinum (Pt), stainless steel (AISI 316L), and textile (silver and copper yarns as conductive material) electrodes. The results show that Ag/AgCl electrodes have the shortest stabilisation time or, alternatively, least noise in the biopotential measurement applications. Stainless steel electrodes also showed good performance in terms of low electrochemical interface noise. It was also verified that all the electrodes will exhibit an equivalent noise level despite of the material as time elapses 10 minutes or more from the application of the electrodes on the electrolyte. Based on the measurement results, optimal materials to be used as electrodes can be determined.

The complex electrode–electrolyte interface can also be expressed as an electrical equivalent circuit model known as the lumped-element model. The model component values were determined from the measurements of some of the electrodes under research in the electrochemical noise measurements. The knowledge about the component values provides means

to calculate the impedance of the electrode which has to be taken into account in designing the measurement amplifier. The interface components also form a natural RC-filter which has to be taken into account when determining the measurement signal bandwidth.

The measurements of the model components were performed with a square wave method, a novel and relatively simple measurement technique. The measurements done in the thesis applied the technique successfully to the component measurements although originally the technique was used for other purposes. The measurement results obeyed the frequency vs. impedance curves widely accepted among scientists.

Some implantable biopotential measurement devices have been designed and realised and the results are reported in the thesis. An inductively powered implantable electrocardiogram (ECG) measurement device is presented and both *in vitro* and *in vivo* measurement results are reported. A resonance-based biopotential measurement device is also introduced. The measurement device has an extremely simple construction and is basically a resonating LC-tank whose impedance is modified by a varactor. The reflected impedance of the LC-tank can be measured at the detector device from which the biopotential can be derived. Measurement results of the human ECG measured from the skin surface with the device are reported in the thesis.

PREFACE

The work presented in the thesis was carried out at Tampere University of Technology (TUT) and more specifically at the Institute of Measurement and Information Technology (–2008) and at the Department of Automation Science and Engineering (2009–) due to structural changes at TUT.

The work towards the dissertation was begun in September 2003, when a project funded by the Academy of Finland was launched. The project, known as TULE (Finnish abbreviation for Future Electronics), introduced an interesting and complex world of implantable medical devices to everyone involved in the project. The problems were many on the bumpy road towards the first prototype of the implantable ECG monitoring device that was tested *in vivo* in cows in summer 2006. However, the project learnt a lot and the author is highly grateful for the Academy of Finland to finance such an interesting project.

In 2006, a new project was launched, called Wisepla, that was funded by the Finnish Funding Agency for Technology and Innovation (TEKES) and several Finnish companies. The new project was focused on surface measurement technology and especially on a wearable, long-term bioimpedance device for cardiac and respiratory measurements. This incorporated textile electrodes into the research. There was, however, further development of the implantable ECG-measurement device going on as well. The project enabled the research group to miniaturise the device. Again, the author is highly grateful for the finance of the project which learnt among other, more technical issues, the author many valuable things about project management.

The department has provided me with the opportunity to write and finish my thesis on its expense. Without this remarkable financial support from the department, the thesis might never have been published or at least it would have been postponed into the future.

I want to express my deepest gratitude to the head of the department, Professor Jouko Halttunen, for kindly providing me the chance to stay a long time at the department and also for proofing my thesis. Professor Jukka Lekkala, my supervisor, deserves a great thanks for his assistance and guidance to get me on the right tracks in the beginning of my doctoral studies and for the guidelines provided by him during the writing period of the thesis. I also want to thank him for getting me involved in the interesting projects and relying on me in the project manager position. Casual discussions with him have also been pleasurable and motivating.

I highly appreciate the work done by the pre-examiners. Professor Danilo De Rossi from University of Pisa and Dr. Tech. Pasi Talonen from Atrotech Ltd. have made excellent and huge job in reviewing the thesis and suggesting improvements and clarifications to the thesis. The work of both gentlemen has both enhanced the level of the thesis and made it more readable.

Overall the people, either currently or previously, working at the institute and the colleagues from other departments, have generated a very friendly and merry atmosphere where it has always been joyful to work in. The people have always been very helpful whenever assistance was needed. I want to express my deepest gratitude to a dear friend of mine, an excellent researcher, M.Sc. Ville Rantanen who has shared the office with me for several years. The sometimes a little bizarre humour we both share has been an asset in the everyday working environment.

The construction of the prototypes for many occasions has been possible thanks to Protopaja, where they could realise the tasks based on my partly unspecific drawings, schematics and explanations. Thanks also belongs to the cleaning ladies in our wing who kept the rooms and corridors clean and tidy thus providing us with a comfortable working environment.

The encouraging attitude and support, towards education provided by my childhood home and parents, both mentally and financially, has played a great role in my decision to begin the dissertation process. I owe a great thanks to them.

The journey that started on a beautiful, yet chilly, September morning in 2003, to the date of dissertation, has been long. However, I have had a great opportunity to share the whole journey with my lovely wife, Jonna. During the dissertation process, our son Eetu has joined the team and delighted us from day to day. The relaxing and loving influence by these two people, has been one of the key factors in my well-being and they have also provided me with insights into the real life outside the work. Although working is undoubtedly an important part of life, the real life I love and respect lies outside the boundaries of the working place and does not care about titles.

Tampere, 14th April 2010
Jarno Riistama

TABLE OF CONTENTS

LIST OF PUBLICATIONS

Parts of the thesis have been previously published. The following publications are included in the thesis.

[P1] Riistama, J. and Lekkala, J. " Electrode-electrolyte Interface Properties in Implantation Conditions," in *Proceedings of the 28th Annual International Conference of the IEEE Engineering in Medicine and Biology Society – EMBC. Engineering Revolution in Biomedicine*, New York City, New York, USA. p. 6021-6024. 30 August—3 September, 2006.

[P2] Riistama, J. and Lekkala, J. "Electrochemical noise properties of different electrode materials in different electrolytes", in Leonhardt, S., Falck, T. & Mähönen, P. (Eds.). *IFMBE Proceedings. Volume 13. 4th International Workshop on Wearable and Implantable Body Sensor Networks (BSN 2007)*, RWTH Aachen University, Germany, pp. 149–154, March 26–28, 2007.

[P3] Riistama, J., Väisänen, J., Heinisuo, S., Lekkala, J., and Kaihilahti, J. "Evaluation of an implantable ECG monitoring device *in vitro* and *in vivo*", in *Proceedings of the 29th Annual International Conference of the IEEE EMBS Engineering in Medicine and Biology Society in conjunction with the Biennial Conference of the French Society of Biological and Medical Engineering (SFGBM)*, Lyon, France. pp. 5703–5706, August 23–26, 2007.

[P4] Riistama, J., Väisänen, J., Heinisuo, S., Harjunpää, H., Arra, S., Kokko, K., Mäntylä, M., Kaihilahti, J., Heino, P., Kellomäki, M., Vainio, O., Vanhala, J., Lekkala, J., and Hyttinen, J. "Wireless and inductively powered implant for measuring electrocardiogram", Medical & Biological Engineering & Computing **45**:1163–1174, 2007.

[P5] Riistama, J., Aittokallio, E., Verho, J. and Lekkala, J. "Totally passive wireless biopotential measurement sensor by utilizing inductively coupled resonance circuits", Sensors and Actuators A – Physical **157**(2):313–321, 2010.

[P6] Riistama, J., Röthlingshöfer, L., Leonhardt, S., and Lekkala, J. "Noise and interface impedance of textile electrodes on simulated skin interface", *submitted to the Journal of IFMBE Medical and Biological Engineering and Computing*, 2010.

SUPPLEMENTARY PUBLICATIONS

The following publications are not included in the thesis but are relevant with respect to the topic and therefore included into the list of supplementary publications.

[P7] Riistama, J. and Lekkala, J. "Characteristic Properties of Implantable Ag/AgCl- and Pt-electrodes," in *Proceedings of the 26th Annual International Confenrence of the IEEE EMBS (Engineering in Medicine and Biology Society)*, San Francisco, California, pp. 2360–2363, 1–5 September, 2004.

[P8] Riistama, J., Lekkala, J., Väisänen, S., Heinisuo, J., and Hyttinen, J. " Introducing a Wireless, Passive and Implantable Device to Measure ECG" in Kneppo, P. & Hozman, J. (eds.) *IFMBE Proceedings. 3rd European Medical & Biological Engineering Conference IFMBE European Conference on Biomedical Engineering EMBEC'05*, vol., 11, International Federation for Medical and Biological Engineering, Prague, Czech Republic, 5 p., 20–25 November, 2005.

[P9] Heinilä, H., Riistama, J., Heino, P., and Lekkala, J. "Low cost miniaturization of an implantable prototype", Circuit World **35**(1):34–40, 2009.

CONTRIBUTION OF THE AUTHOR

In publications P1, P2 and P7 the author has been the main author of the papers. The author has also designed the measurement methods, conducted the measurements and analysed the measurement results.

In publications P3, P4 and P8 the author has been the main author of the paper. The author has also participated in the designing, construction and testing of the implantable ECG measurement devices as well as the data analysis.

In publication P5, the author has been the main author of the paper and made also data analysis on the measurement data. The author has actively participated in the supervision of a M.Sc. thesis regarding the matters discussed in the paper.

In publication P6, the author has been the main author of the publication, designed the measurement methods and conducted the measurements. Materials used in the measurements together with the corresponding chapters in the publication were supplied by Ms Röthlingshöfer.

Publication P9 is mainly written by Ms Heinilä. The author has participated in the designing process of the implantable device, conducted the *in vivo* measurements, analysed the results and written the consecutive part in the publication.

LIST OF ABBREVIATIONS

AC	Alternating current
Ag	Chemical symbol for silver
AgCl	Chemical symbol for silver-chloride compound
AISI316L	Acid resistant stainless steel
Au	Chemical symbol for gold
BP	Blood pressure
CMRR	Common mode rejection ratio
DAQ	Data acquisition
DC	Direct current
ECG	Electrocardiogram, graph describing the electrical activity of the heart
EEG	Electroencephalogram, graph describing the electrical activity of the brain
EIS	Electrochemical impedance spectroscopy
FEM	Finite element method
FFT	Fast Fourier transform
Hg	Chemical symbol for mercury
HRV	Heart rate variability
IC	Integrated circuit
ICA	Independent component analysis
IDT	Interdigital transducer
ILR	Implantable loop recorder

LSK	Load shift keying
MEMS	Micro electro mechanical systems
PBS	Phosphate buffered saline
PCA	Principal component analysis
PCB	Printed circuit board
Pt	Chemical symbol for platinum
RF	Radio frequency
RMS	Root-mean-square
SATP	Standard ambient temperature and pressure, $T = 25\,^{\circ}\mathrm{C}$, $p = 1$ atm
SAW	Surface acoustic wave
SBF	Simulated body fluid
SNR	Signal-to-noise ratio
Ti	Chemical symbol for titanium
TUT	Tampere University of Technology
TWB	Total Water Balance
VCO	Voltage Controlled Oscillator

LIST OF SYMBOLS

A	Anion molecule of an electrolyte
A	Gain of an amplifier
A_{cm}	Amplifier common mode gain
A_{d}	Amplifier differential gain
A_{e}	Confronting area of electrodes
A^{n-}	Anion molecule of an electrolyte with valence n
A_T	Auxiliary variable used in the electrode impedance analysis
a_{ox}	Activity of the oxidised agent
a_{red}	Activity of the reduced agent
α	Auxiliary variable used in the electrode impedance analysis
C	Correlation coefficient between amplifier voltage and current noise
C_{c}	Parallel capacitance of the skin contact
C_{H}	Capacitance of the double layer
C_i	Fixed capacitance of a resonance sensor with $i = 1, 2, 3, \mathrm{k}$
C_{p}	Capacitance over electrode–electrolytic gel interface
$C_{\mathrm{d}}^{\mathrm{p}}$	Diffusion induced capacitance of the double layer in parallel circuit presentation
$C_{\mathrm{p,d}}$	Parallel capacitance of the dermis
$C_{\mathrm{p,e}}$	Parallel capacitance of the epidermis
$C_{\mathrm{p,s}}$	Parallel capacitance of fibrous sheath
$C_{\mathrm{p,t}}$	Parallel capacitance of tissue

$C_{\mathrm{d}}^{\mathrm{s}}$	Diffusion induced capacitance of the double layer in series circuit presentation
$D_{(i)}$	Capacitance diode of a resonance sensor with i = 1, 2, or with no sub index
δ	Thickness of the compact layer
E_i	Non-equilibrium potential caused by a current flow
E_0	Standard potential under SATP conditions
η	Overpotential of an electrode
F	The Faraday constant, $F = 9.6487 \cdot 10^4$ C/mol
Δf	Frequency step in a discrete spectrum
I_F	Auxiliary variable used in the electrode impedance analysis
$I_{\mathrm{n,\,a}}$	Current noise of an amplifier
I_S	Auxiliary variable used in the electrode impedance analysis
$I_U(t)$	Faradic current through measurement resistor at time instant (t)
$L_{(i)}$	Inductance of a resonance sensor with i =1, 2 or with no sub index
l	Separation of electrodes
M	Metallic atom of an electrode
M^{n+}	Metallic ion of an electrode with valence n
n	Valence of a redox reaction
$n(e^-)$	Number of electrons
$p_{\mathrm{H_2}}$	Partial pressure of hydrogen
R	Molar gas constant, $R = 8.314$ J/(K·mol)
R_{B}	Polarisation resistance of the bulk electrolyte
R_{c}	Parallel resistance of the skin contact
R_{G}	Resistance of electrolytic gel
R_i	Resistance of a resonance sensor with i =1, 2
R_{lead}	Resistance of the measurement lead

R_{meas}	Resistance of the measurement resistor
R_{p}	Charge transfer resistance at electrode–electrolytic gel interface
$R_{\mathrm{d}}^{\mathrm{p}}$	Diffusion induced resistance of the double layer in parallel circuit presentation
$R_{\mathrm{p,d}}$	Parallel resistance of the dermis
$R_{\mathrm{p,e}}$	Parallel resistance of the epidermis
$R_{\mathrm{p,s}}$	Parallel resistance of fibrous sheath
$R_{\mathrm{p,t}}$	Parallel resistance of tissue
R_{S}	Sum resistance of R_{x} and R_{meas}
$R_{\mathrm{d}}^{\mathrm{s}}$	Diffusion induced resistance of the double layer in series circuit presentation
R_{T}	Resistance of tissue
R_{t}	Charge transfer resistance of the double layer
R_{x}	Volume resistance of electrolyte in impedance measurements
ρ	Resistivity of an electrolyte
T	Absolute temperature
T	Half period of a square wave
ΔT	Time step, $\Delta T = T/8$
V_{BIO}	Biopotential voltage
$V_{\mathrm{n},i}$	$i =$ e,a: voltage noise of an electrode or amplifier respectively
$V_{\mathrm{n,T}}$	Total equivalent noise of an amplifier–electrode circuit
V_{re}	Voltage reduced to electrodes
V_{S}	Square wave voltage source amplitude
$v_{\mathrm{rms}}^{\mathrm{f}}$	RMS noise calculated from a discrete voltage spectrum
$v_{i,\mathrm{f}}$	Voltage density of the i:th component in a discrete voltage spectrum
$v_{\mathrm{in},i}$	Input voltage of an amplifier with $i = 1, 2$
v_{out}	Output voltage of an amplifier

X_2	Reflected impedance of a resonance sensor
Z_e	Impedance of the electrode–electrolyte interface

1. INTRODUCTION

Monitoring of people during their everyday life or sport performances has increased enormously in the 21st century. The need for the monitoring has arisen either from the suspected or recognised problems in the personal health status or part of the needs may be man-made and arise from the availability of such measurement devices. The wireless heart rate monitors have enabled continuous measurement of cardiovascular events in real time and with little discomfort to the measurement subject. Today, there are several commercial wireless heart rate monitors available on the market and the first such product was made by the Finnish company Polar Electro in 1983. The product was known as Polar Sport Tester PE 2000 [61].

The wearable heart rate monitors are positioned for the mass market and typically the only information available from them is the heart rate. For the medical use, there are devices that are able to measure also the complete electrocardiographic (ECG) cycle and to store it for later analysis. These devices are called Holter monitors and event (loop) recorders [40]. They can capture and store measurement data from the abnormal seizure moments that are not otherwise easily accessed due to their random nature. This helps the doctor to determine the correct treatment methods for the patient.

Other wearable devices that monitor the well-being of the subject have also been suggested. Devices that measure the impedance of the tissues, known as bioimpedance measurement devices, can be used to measure the Total Water Balance (TWB) of a subject [44]. The bioimpedance measurement can also be used to measure e.g. respiration rate and volume [108].

As the number of elderly people is gradually increasing, there is a demand for wearable, wireless measurement devices that are able to monitor the people during their everyday activities. The body water balance is one of the key variables to be monitored in the elderly people where the risk of dehydration is actual [71].

The key demands can be stated shortly for the ambulatory measurement devices that are used to measure physiological signals: In general, they shall be wireless and lightweight. In the development process, certain conventional solutions are sometimes blindly applied although it might be beneficial to consider the basics and explore different alternatives to be used for example as electrode material. Carbon loaded rubber, presented e.g. in [79], is a traditional electrode material to be used in the wearable applications. Electrodes made of textile

materials are, however, emerging thanks to their better integrability into clothing. Examples of textile based electrodes integrated into garment are reported in several publications [44, 84, 87, 90].

The aim in the measurement applications is to obtain good enough signals for the current application with minimal cost and discomfort to the patient. These demands limit the selection of electrode materials, sizes etc. in different ways and the electrode is often a compromised solution between price, size, durability, usability etc. It is of great importance that general information which defines the electrical properties of the electrodes possibly in various applications can be provided.

Some of the surface measurement devices can be made implantable, that is, placed under the skin, to enhance their usability and wearability. With implanted devices, e.g. the pacemakers, the battery and its capacity limits the usability of these devices. The implantable devices can also be powered up wirelessly using inductive coupling between the implanted unit and an external unit on the skin surface. The inductive power coupling needs an external coil on the skin surface whose optimal placement with respect to the implanted receiver coil can be a problem in some cases. Inductively powered measurement devices solve the problem of energy capacity. The inductive power supply method has been used in many applications, e.g. in a phrenic nerve stimulator [116], in an implantable electroencephalography (EEG) monitor [46], an implantable telemetry system for sympathetic nerve activity and ECG measurement system [23].

Making the measurement devices to run on battery makes them more tolerant to interferences. The power line interference, for example, is a smaller problem with battery operated devices than with AC-powered devices since they can float in any potential and thus no common ground is present where the interferences are prone to connect.

The following questions were studied in the thesis:

1. Which electrode materials have the best characteristics in surface and implantable applications? Electrodes exhibiting least electrochemical noise arising from the interface together with low a impedance connection to the tissue or skin, are preferable in most applications. This question is studied and answered in Section 3.3.1.

2. Does there exist other, simpler, methods to measure the parameters of the electrode–electrolyte interface than traditionally used techniques requiring special instrumentation and arrangements? The question is theoretically discussed in Section 2.8 and verified with measurements in Section 3.3.2.

3. Is it possible to obtain reliable long term data from an implantable measurement device? Measurement data loss may be an issue with implantable devices, and also the data is obtained from different environment than with traditional devices so that the

interpretation of it is more difficult. A developed implantable measurement device together with measurement results obtained with the device are presented in Section 4.3.

4. Is it possible to measure bioelectric signals from the skin surface with a minimally complex device? A small, lightweight and inexpensive device that measures the ECG from the skin is under research. Section 4.4 presents the design of such a device together with some preliminary measurement results.

1.1 Structure of the thesis

The thesis contains the following parts:

First, the electrode–electrolyte interface is reviewed. The electrochemical reactions, formation and structure of the double layer, various interface models and artefacts of the measurement signals originating from the interface are discussed in detail. After discussing the interface properties, the measurement methods of the interface electrochemical noise and impedance are presented. There are naturally a number of measurement techniques but only techniques relevant to this thesis are presented.

In the next part, physiological surface measurement devices are discussed first in general and then the results of the electrode characterisation studies are presented. The results are based on the measurements of the author and are also presented in publications P1, P2, P6 and P7.

The following section deals with implantable physiological measurement devices. First some applications are reviewed to provide the reader with an overview of the problem field. Then some characteristic properties and demands of the measurement devices are discussed. After these, the implantable ECG measurement devices designed and constructed at Tampere University of Technology (TUT) are presented. The general presentation of the devices has been divided into a separate section than the measurement results, both *in vitro* and *in vivo*, which are presented in the consecutive sections. These results are also discussed in P3, P4, P8 and P9. The separation of the results from the general presentation of the developed devices is done for clarity of the thesis structure. A totally passive resonant-based ECG measurement device is also presented in this part due to its obvious advantages in implantable applications. The resonant sensor is originally discussed in publication P5. Fig 1.1 presents the interconnections between the different issues investigated and presented in the thesis.

In the end, there is a discussion part included which considers the problems and limitations of the applied measurement methods and debates the implantable ECG measurement devices and their applicability. Conclusions of the obtained results are also presented.

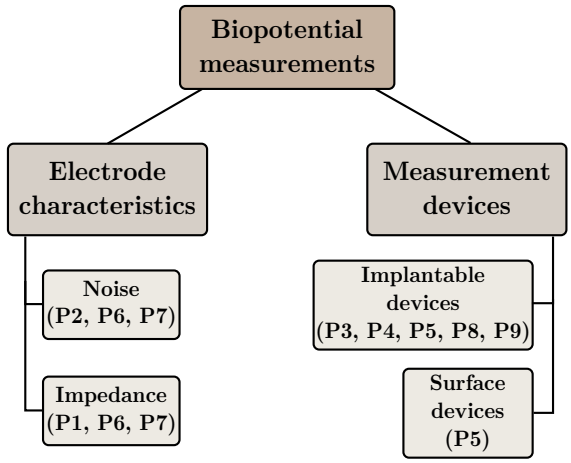

Fig. 1.1. *A schematic figure of the interconnections between different issues researched and presented in the thesis.*

1.2 Contribution of the thesis

Several different electrode materials, both metallic and textile, have been investigated in terms of the electrochemical noise they exhibit at the interface between the electrode and the electrolyte. Several different electrolytes with different electrical conductivities have been used to conduct the measurements, which reflect the differences in the measurement results in several electrolytes.

The thesis presents and verifies a new measurement method for the interface impedance measurement of the electrode–electrolyte interface. The suggested square wave method has been originally presented to be used for measurement of the electrolyte resistance at different frequencies but in the thesis it has been proved that the method can also be successfully applied to the measurement of the interface component values at different frequencies. The thesis contributes to the characterisation of the electrodes with the measurements and analysis of the results with respect to applications. The application aspect in the analysis of the measurement results has often been neglected in scientifical context.

An inductively powered, wireless, implantable measurement device to measure ECG has been presented and tested both *in vitro* and *in vivo*. *In vivo* measurements have been performed in cows, and the results seem promising in terms of applicability of the measurement method and apparatus to animal measurements. The presentation of the devices and the measurements performed with them give much valuable information about the implantable technology and practical knowledge about the applications.

A simple, inexpensive, wireless measurement device to measure biopotentials has been introduced. Test measurements of ECG signal have been made with the device from the skin

surface and the device has been found to be applicable to biopotential measurements. The device presents a fairly new measurement method that can be made affordable and disposable. Furthermore, the measurement device can be used on the skin surface or as implanted which makes it even a more important application.

In addition, the thesis gathers the widespread information, and generates new one, on the various electrode materials, electrolytes and their behaviour in one volume and connects the theoretical aspects of the electrode characteristics with the real-life applications.

2. ELECTRODE-ELECTROLYTE INTERFACE

The interface between the metallic electrode and ionic electrolyte is a complex system. Electrochemical reactions, section 2.1, occur at the interface which cause current to flow through the interface. There are two kinds of currents: displacement current originating from the displacement of charge carriers at the interface region and faradic current due to charge transfer through the interface. The displacement current can also be called as a capacitive current. The faradic current is caused by redox reactions taking place at the interface. The reactions can either release ions of the electrode into the solution or vice versa. [14, 28, 126] Fig 2.1 visualises the structure and relations of the electrode–electrolyte interface that are discussed in more detail in the consecutive sections.

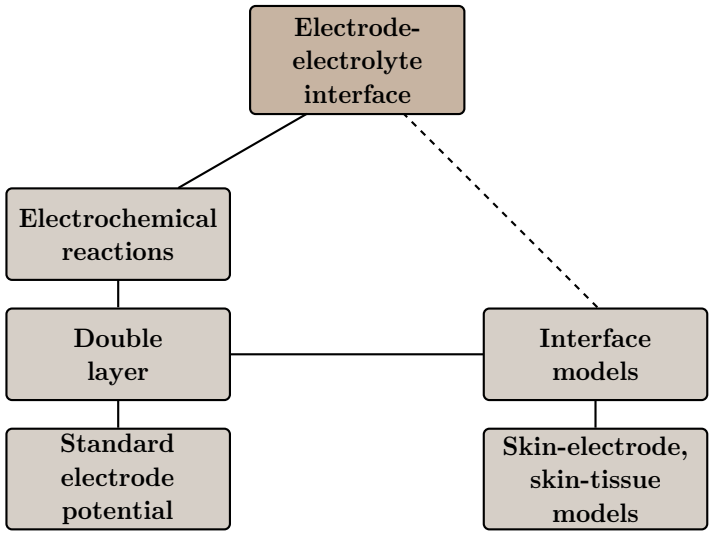

Fig. 2.1. *Structure and relations of the electrode–electrolyte interface.*

2.1 Electrochemical reactions

When an electrode is immersed in an electrolyte, the electrochemical reactions on the electrode surface begin immediately. In the electrode, the current is carried by the electrons

whereas in the electrolyte the free ions of the substance act as charge carriers. For the current to be able to flow through the electrolyte to the electrode and further to measurement electronics, a charge transfer has to occur at the electrode–electrolyte interface.

When the metallic electrode is introduced into the electrolyte and a current should flow through it, either an oxidation reaction of the electrode atoms or a reduction/oxidation reaction of the electrolyte ions will occur. The reaction type of the electrolyte will depend on the polarisation of the ions in the electrolyte. The reaction when the metallic atoms of the electrode are oxidised can be stated as follows:

$$M \rightleftharpoons M^{n+} + n(e^-) \tag{2.1}$$

where M represents the metal atom, n its valence (integer), e^- an electron and $n(e^-)$ number of electrodes. For the case when reduction/oxidation of the electrolyte ions is to occur, the reaction will be written as:

$$A^{n-} \rightleftharpoons A + n(e^-) \tag{2.2}$$

where A^{n-} represents an anion atom or molecule of the electrolyte solution and A is the atom or molecule of the electrolyte. The reduction/oxidation reactions are normally abbreviated as redox reactions [9].

The redox reactions taking place at the electrode–electrolyte interface will cause the charge distribution at the interface to differ from that of the rest of the electrolyte. The charge accumulation at the interface can be measured as higher potential at the electrode than in the bulk electrolyte. This potential difference is known as half cell potential and the layer with a high charge density at the interface is called a double layer.

2.2 Double layer

The double layer has been discussed among the scientists in the electrochemical field since 1879 when Helmholtz for the first time suggested that such a layer exists. The double layer is formed at the interface between the electrode and electrolyte due to the charge accumulation. The charge is accumulated on the interface because of the redox reactions described in subsection 2.1.

There exist several double layer models. Typically, the models have evolved as the time has passed and knowledge and instrumentation have been developed yielding the newer models to be more complex than the older ones.

The first model suggested by Helmholtz in 1879, Fig 2.2(a) was relying on assumption that on the surface of the metallic electrode there exists a tight layer of charges (positive metal ions) and an equally tight layer of oppositely polarised charges are located in the electrolyte on the surface of the electrode. Helmholtz estimated that the separation between the two

layers would be measured in molecular dimensions. The layer was called the *space-charge region*. [14, 28]

However, the Helmholtz model did not satisfactorily describe the electrode–electrolyte interface. In 1910, Gouy suggested that the creation of the double layer was also depending on the osmotic pressure of the ions in the electrolyte. This lead to a smoother, exponentially decaying potential distribution, Fig 2.2(b). Later, in 1913, Chapman further suggested that the osmotic pressure of the ions is equal in strength with the electrostatic force that the charges exhibit. [126]

In 1924, Stern suggested yet another structure for the space-charge region, Fig 2.2(c). This model was a more comprehensive model from those of Helmholtz's or Gouy's. The Stern model divided the space-charge region into two parts. A *compact* layer of charge is formed by the ions closest to the electrode surface. The strong electrostatic forces bind the ions tightly to the layer. The thickness of the compact layer is roughly the radius of a hydrated ion. Another part is a *diffuse* layer that extends further to the electrolyte and where the ions are more loosely arranged than in the compact layer. The dimension of the diffuse layer is in the range of tens of ångstroms (Å) and depends on the concentration of the electrolyte. As the concentration increases, the length of the diffusion layer decreases. [14]

Stern extended his model further to include cases where the electrolyte contains dipoles. The ions bound to the electrode surface that form the compact layer have a minimum distance from each other. The gaps between the ions can be filled by the small dipoles and the potential curve will be as shown in Fig 2.2(d). [126]

2.3 Standard electrode potential

The double layer created at the electrode–electrolyte interface also creates a charge distribution at the interface with a non-zero total charge. Hence, a potential is acting at the interface. The potential is known as the *half cell* potential or the *standard potential*. The potential depends at least on the temperature, electrode material, electrolyte and pH of the electrolyte. [14, 28]

A reference potential is needed in measuring the standard potential of an electrode. Therefore, another electrode is needed and the measured potential is the difference of these two electrodes. However, every metallic electrode exhibits a potential of its own and the measured differential potential is not revealing the nature of the electrode under test unless a common reference potential is defined.

According to an international agreement, the standard potential of a hydrogen electrode has been defined to be zero when the following circumstances apply: The hydrogen electrode consists of a platinum electrode with electrodeposited platinum black and it is immersed in

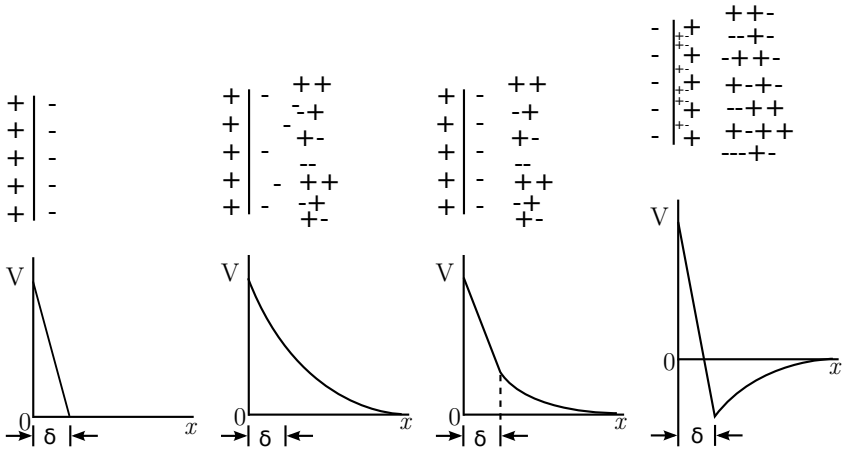

(a) Helmholtz model, 1879 (b) Gouy model, 1910 (c) Stern model, 1924 (d) Stern model with dipoles, 1924

Fig. 2.2. *Various electrode–electrolyte interface models named after their inventors and years.* δ*, in the distance from the electrode vs. potential figures, denotes the thickness of the compact layer in each case.*

an acid. When the activity of a hydrogen ion in the acid is 1 mole/litre (pH=0) and hydrogen gas is bubbled around the electrode while its partial pressure p_{H_2} is 1 atm, the standard potential of this electrode type is defined to be zero at all temperatures. The reason for the hydrogen electrode to be chosen as the universal reference electrode lies in its reproducibility and stability. [14] The hydrogen electrodes can be produced so that the potential difference of two hydrogen electrodes is less than 10 μV while for other electrodes the potential variations are typically measured in the order of mV. The saturated calomel electrode (SCE with Hg–Hg_2Cl_2) is however comparable in stability and reproducibility with the hydrogen electrode. The potential variations of 1-20 μV have been measured for the SCE. [14, 28]

The standard potential of all other electrode materials is measured against the hydrogen electrode prepared in the manner explained earlier. The standard potential values measured and tabulated e.g. in [14, 28] are measured against the hydrogen electrode but under SATP conditions (SATP = Standard athmospheric temperature and pressure, $T = 25\,^{\circ}\mathrm{C}$, $p = 1$ atm.). The potentials will therefore be modified when either the temperature, electrolyte or pH of the electrolyte changes. The standard potential modified by the temperature changes obey the Nernst equation

$$E_i = E_0 + \frac{RT}{nF} \ln\left(\frac{a_{\mathrm{ox}}}{a_{\mathrm{red}}}\right) \tag{2.3}$$

where E_0 is the standard potential in SATP conditions, R molar gas constant, T the absolute temperature, n the number of exchanged unity charges, F the Faraday constant and a_i the activities of reduced and oxidised species respectively.

The standard potential applies only when the electrode is in electrochemical equilibrium with the electrolyte and no current is drawn from the system. In the real life measurements, immediately when the electrode comes into contact with the body, a current begins to flow through the electrode and the potential difference over the interface will change. There have been identified four different reasons for the potential variation: [14, 52, 126]

1. charge transfer process through the electrode double layer
2. diffusion caused by concentration gradient or field
3. chemical reaction limiting the electrode reaction
4. crystallisation of the metal ions at the interface.

The difference between the disturbed potential and the standard potential is called overpotential, η, and can be formulated as

$$\eta = E_i - E_0 \tag{2.4}$$

where E_i is the non-equilibrium potential caused by the current flow. E_i is a function of applied current density that flows through the electrode. The theory behind the four previously mentioned overpotential contributions is complex and since it is not the focus of this thesis, it is omitted here. For more exact discussion about these overpotential methods references [14, 126] are advised to be read.

When η is close to or exactly zero, the electrode is said to be non-polarisable and otherwise polarised. The concept of polarisation of the electrode is misleadingly two-folded. One of the interpretations is as discussed previously and another suggested by Parsons in 1964 is related to the charge exchange in the double layer. According to the other definition, the perfectly polarised electrode does not change charge over the interface whereas for the perfectly non-polarisable electrodes there is a free exchange of charge over the interface. Real life electrodes lie in between these extremities. Ag/AgCl-electrodes are close to being perfectly non-polarisable and Pt electrodes lie close to the other end. [92]

2.4 Interface models

The double layer at the electrode–electrolyte interface has charges of one polarity on one side and oppositely polarised charges on the other side of the interface. Hence, an intrinsic capacitor is formed over the layer. When an electrical equivalent of the double layer is being formulated, the resulting capacitor has to be included in the model. The standard potential acting over the interface adds a voltage source to the model. Yet it is known that also direct current can flow through the interface, hence a resistor also has its place in the model. [28]

Although the determination of the components comprising the electrical equivalent of the double layer (also known as the *lumped element model*) is somewhat straightforward, the determination of the connections between them has not always been clear. The determination of the component values is also a challenging task since the values are affected by the electrode metal, its area, electrolyte, temperature, current density and the frequency of the current used in the measurement situation. [14, 28]

In the case, where the charge transfer process is the most dominating part of the electrode overpotential, the electrical equivalent of the interface is straightforward: a parallel connected resistor and a capacitor, Fig 2.3(a). The capacitance C_{H} represents the capacitance of the double layer and R_{t} represent the resistance caused by the charge transfer at the interface. This approximation of the interface is valid under small signal conditions, i.e. when the current density remains at low level. [14, 30, 126] The model is a special case of the standard Randles equivalent circuit originally presented in [97].

For an electrode material for which the exchange current density is low, the charge transfer overpotential is the dominating part of η. An example of such a material is Pt in hydrogen whereas for Ag the effect of charge transfer overpotential is negligible. [14]

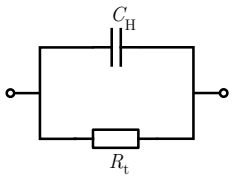

(a) Electrical equivalent ignoring diffusion mechanisms.

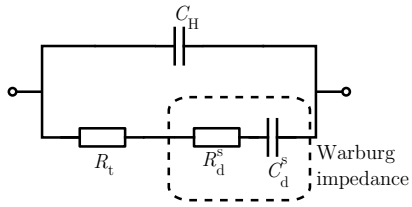

(b) Equivalent circuit with Warburg series component.

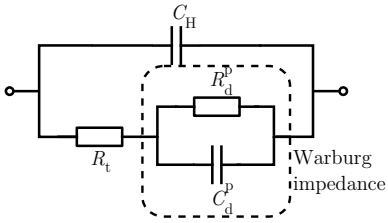

(c) Equivalent circuit with Warburg parallel component.

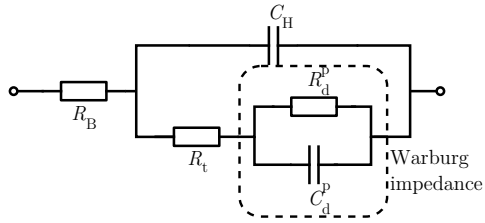

(d) Equivalent circuit with Warburg parallel component and electrolyte bulk resistance.

Fig. 2.3. *Evolution of electrical equivalent circuits of the electrode–electrolyte interface.*

Warburg was the first to analyse the overpotential caused by the diffusion mechanisms under a sinusoidal excitation current. The sinusoidal current applied over the electrode will cause the charge concentration to vary as a function of time at the interface. The charge den-

sity fluctuations can be regarded as concentration waves propagating in the electrolyte. The concentration wave amplitude will be decreased by the damping of the electrolyte and the spreading of the wave as it propagates in the electrolyte. It is possible to define a penetration depth for the concentration wave. At the distance of penetration depth from the electrode interface the amplitude of the concentration wave is $1/e$ of the initial amplitude at the electrode. When the frequency of the sinusoidal signal increases, also the damping increases thus causing the penetration depth to decrease. This leads to situation where eventually the concentration wave will only be in the proximity of the electrode surface. When the penetration depth is much smaller than the diffusion layer thickness, the impedance caused by the diffusion will be negligible. Then the electrical equivalent of the interface will be like in Fig 2.3(b) or its parallel equivalent in Fig 2.3(c).

The component names R_{d}^{i} and C_{d}^{i} in Fig 2.3(b) and Fig 2.3(c) with $i = \mathrm{p}, \mathrm{s}$, represent the diffusion induced resistance and capacitance. They are both inversely proportional to the square root of the applied signal frequency [30]. This fact makes it reasonable that the impedance of the circuit presented in Fig 2.3(b) will be close to zero when the frequency is sufficiently high. On the contrary, the impedance will be infinite if the frequency approaches zero. In this case, a frequency independent value for the Warburg impedance can be defined which keeps the impedance finite.

The model of Fig 2.3(b) can be converted to a parallel connected resistor–capacitor model. The component values have to be scaled yet the same frequency behaviour applies. The parallel connected Warburg equivalent circuit is presented in Fig 2.3(c).

The polarisation resistance of the bulk electrolyte can be easily added to the interface model by adding an ohmic resistance R_{B} in series with the circuit equivalent, see Fig 2.3(d). The same addition can be made for all presented circuit equivalents and by adding it to circuit Fig 2.3(a), the Randles equivalent circuit is formed. Geddes and Baker suggested in [28] that the half cell potential can be added to the electrical equivalent as a DC-voltage source.

The electrical equivalent circuit shown in Fig 2.3(d) is the most complex and comprehensive electrical equivalent circuit model. The model can, however, be simplified when both low frequency and high frequency behaviour is examined. For the low frequency signals, the behaviour of the double layer is dominated by the Warburg circuit component and the circuit can be effectively reduced to contain only the Warburg impedance, Fig 2.4(a). [14]

When high frequency signals are considered, the Warburg impedance will be negligible since both components of the Warburg model are inversely proportional to the applied frequency. Thus the interface impedance is dominated by the double layer capacitance and the electrolyte resistance. The high frequency approximation of the interface electrical equivalent is as in Fig 2.4(b). [14]

The electrical equivalent component values of the interface also exhibit frequency depen-

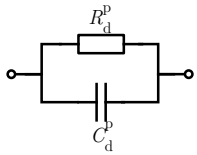

(a) Low frequency approximation of the electrical equivalent circuit of the electrode–electrolyte interface.

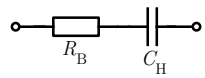

(b) High frequency approximation of the electrical equivalent circuit.

Fig. 2.4. *Low and high frequency approximations of the electrode–electrolyte interface electrical equivalent circuits.*

dency. It has been suggested and with measurements proved that the interface component values are exponentially decaying with frequency. There have been various suggestions on whether both the resistance and the capacitance in model illustrated in Fig 2.3(a) would show the same frequency dependency or should they be separated from each other having decay constants of their own. The theory that is more widely used and proved correct, e.g. in [14], suggests that both the components have independent decay constants. [14, 28, 30, 103, 126]

Bera *et al.* have concluded in their study that by superimposing DC and AC current in the measurement of interface parameters produce more reliable information about the polarisation impedance for natural biosignals that contain both the DC and AC components. They also observed that the interface component values show a transition point where the decay constants of both the resistance and the capacitance are altered. The behaviour was suggested to happen due to the usage of the DC current in the measurement. [7]

Schwan reported in [104] that the current density used for either measurement or simulation through the electrodes has a significant effect on the interface values the system exhibits. He measured the interface component values of the interface model shown in Fig 2.3(a) for a Pt electrode in KCl solution. The measurement frequency used was 100 Hz, electrode area nearly 1 cm^2 and the nonlinear range begun from current value 0.4 mA which corresponds to current density of approximately 0.4 $\mathrm{mA/cm}^2$. The non-linearity will be shown in the interface resistance as rapidly decreasing values with increasing current density. For the interface capacitance, the effect will be opposite.

In his article, Schwan suggested that the limiting current density shall be assigned a value that corresponds the current density at which a 10 % deviation of the interface component values, R_{t} and C_{H}, from their small signal values, is detected. He also suggested that the relationship of the limiting current with frequency would follow an exponentially increasing form with an exponential constant of the same absolute value as the capacitance of the corresponding electrode material–electrolyte interface has. This means that the limiting current of linearity

is higher at higher frequencies. [103]

McAdams *et al.* have also reported of the current limits for linear behaviour of the interface component values [65]. In their article it is suggested that the parallel connected resistor–capacitor model of Fig 2.3(a) is an appropriate model to be used in the modelling of the electrode–electrolyte interface. They also state that the charge transfer resistance, R_t, dominates the impedance of the system at the low frequency zone and the nonlinear behaviour is first seen in the value of this component. When the frequency is increased, the capacitance will be more dominant and the non-linearity will also be seen in those values.

Recently, Oh *et al.* have studied electrode systems with nanoscale gaps. They have reported results where the influence of the electrode polarisation impedance on the measurement results can be remarkably reduced by a nanometer scale gap between the electrodes, which causes the double layers of the electrodes to overlap. The gap between the electrodes was held much under 100 nm and the variations in the capacitance and resistance were mainly caused by the sample solution. [85]

It is impossible to define exact universal interface component values for the components presented in Fig 2.3(d). This is because in realistic measurement situations, the applied frequency of the signals vary as well as the current through the electrodes. Since all the component values are dependent on the frequency and current density, the component values are constantly changing. The information band e.g. of the ECG signal lies between 0.5–40 Hz and the signal waveform has a varying amplitude which implies also varying current density at the electrodes during ECG measurements [114].

The resistance and the capacitance appearing in the interface models cause deformations in the measurement signals since the interface will act like an RC-filter. It is therefore important that the interface values are such that the signal to be measured is not drastically modified by the interface properties. [14]

2.5 Skin-electrode and skin-tissue interface models

The electrical equivalents of interfaces at pure electrode–electrolyte interface are as shown in Fig 2.3 and in Fig 2.4. However, when the electrodes are used in real measurement applications, e.g. on the skin, there will be several interfaces on the signal route beginning from the signal source and ending at the electrode and read-out electronics. Furthermore, the interfaces are different for widely used gel-paste electrodes, textile electrodes and implantable electrodes. The interfaces of all these three situations are illustrated in Fig 2.5. The schematic graphs have been modified from sources [67, 70].

Components and their values in Fig 2.5(a), which describes the measurement setup for a standard electrolytic gel enhanced electrode, denote the resistance of the leads connecting

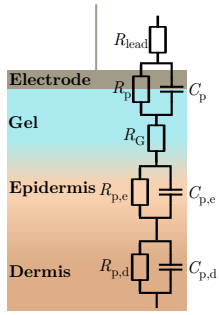

(a) Electrical equivalent circuit of the electrode–electrolyte interface for a gel-paste electrode on skin.

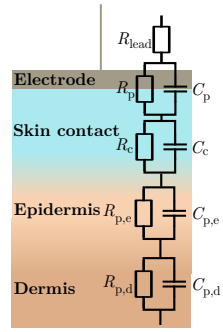

(b) Electrical equivalent circuit of the electrode–electrolyte interface for a textile electrode on skin.

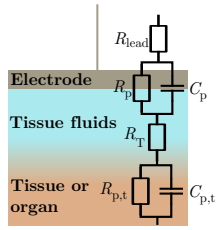

(c) Electrical equivalent circuit of the electrode–electrolyte interface for an implantable electrode.

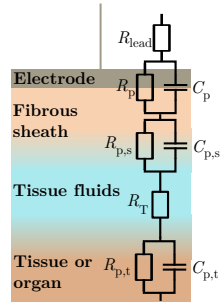

(d) Electrical equivalent circuit of the electrode–electrolyte interface for an implantable electrode with a fibrous sheath.

Fig. 2.5. *Electrode–electrolyte interface electrical equivalent circuits for various electrode types. Figures modified from [67, 70]*

the measurement electronics to the electrode (R_{lead}), the simplified interface impedance of the electrode–ion based conducting media (R_{p} and C_{p}), the impedance of the conducting electrolytic gel applied between the electrode and the skin (R_{G}), which is mostly resistive and the impedance of the epidermis (the outer layer of the skin) and dermis (deeper layers of the skin not, however, including the subcutaneous tissues). The usage of the Randles model is acceptable since in measurement applications, the current density is inherently kept at a low level.

For the case of a textile electrode, Fig 2.5(b), the situation is otherwise similar except from the connecting layer between the electrode and the skin. When textile electrodes are being used,

it is desirable that no electrolytic gel is needed to enhance the electrical connection between the electrode and skin. Therefore, especially shortly after application of the electrodes on the skin, the connection is highly capacitive which is introduced into the model by capacitor C_c. After some time, sweat and humidity create an alternative, resistive, route for the current represented by R_c. [70]

For the case of an implantable electrode, the skin layers are totally missing and around the electrode there is possibly only a small amount of tissue fluids between the signal source (tissues) and the electrode. The tissue fluids have a high ion concentration and thus the impedance of this layer is almost purely resistive (R_T). The tissue interface is located immediately after the tissue fluids and the capacitive element ($C_{p,t}$) has been added for convenience to cover the electrical properties of several possible tissues (e.g. muscle and fat).

In a review article by van Kuyck *et al.* [124], the effect of long term implantation of the electrodes to the surrounding tissues is reviewed. The article gathers information from 26 autopsy studies mainly from the 1970's and 1980's, where electrodes have been used to stimulate the human brains. The studies reveal that the stimulation waveform has a remarkable effect on the damage the stimulation causes to the surrounding tissue. Usage of biphasic stimulation pulses has been proved to be better to the tissues in terms of low probability for lesions in the target area. In some cases, hemorrhage was observed at the implantation site which was deduced to be caused by the implantation itself. [124]

Hemorrhage or other type of lesion at the site of the electrode will enhance the effect of the tissue fluid layer due to high electrical conductivity of blood. In contrary to the well conducting tissue fluid layer, according to the experiments, it was also noticed that a fibrous sheath was formed at the electrode–tissue interface. This was not, however, the case in every study. The formation of the fibrous sheath was not dependent on the electrode being a stimulating or non-stimulating (recording) electrode. If the sheath was to be formed, it was observed that the thickness of the sheath was directly proportional to the charge density during one stimulation pulse. [124]

The fibrous sheath is by nature strongly non-conducting tissue but in some experiments it was found to be highly vascularised. [124] This makes the sheath to conduct both capacitive and resistive nature ($R_{p,s}$ and $C_{p,s}$). Hence, another layer will be formed between the electrode and the tissue fluid layer whose electrical properties are dominated by the capacitive nature of the fibrous sheath yet some resistive nature still exists depending on the degree of vascularisation of the tissue, see Fig 2.5(d). The thickness of the sheath is in the range of tens of μm:s [102].

2.6 Artefacts of the electrodes

The biopotential measurements typically suffer from various kinds of artefacts affecting the measurement signal. Examples of such artefacts are e.g. motion artefacts, artefacts caused by different biopotential signals than the desired, typically EMG signals, and artefacts due to electrochemical noise at the electrode interface. [13, 28]

The double layer is the source of the motion induced artefact. The charge distribution at the interface is disturbed as the electrode moves with respect to skin. [9, 28]

There are several techniques to reduce the motion induced artefacts. One simple technique is to choose the placement of the electrodes so that they are located on places where the interface movements between the electrode and skin are at minimum. One such application is presented by Qu *et al.* in [96]. They conducted impedance cardiography measurements with spot electrodes instead of the traditionally used band electrodes. A better signal-to-noise ratio (SNR) was obtained with the spot electrodes due to smaller movement artefacts in the signal.

The effect of motion artefact on the measurement result can also be reduced by using electrodes of recessed type. The recessed type electrodes do not have a direct connection to the skin. Instead, they are connected to the skin via an interface medium. Nowadays, there is typically a layer of conductive hydrogel paste added around the electrode which will stabilise the electrode–electrolyte interface and reduce the motion artefacts. [30, 52]

The varying contact pressure also causes artefacts to the measurement signal. The artefacts due to varying contact pressure will be represented in the measurement signal as the motion induced artefacts. Degen *et al.* have studied the possibility to reduce these artefacts by measuring the impedance of the electrode–electrolyte interface [18]. The method is not novel as such but in controversy to the other similar methods, the proposed method does not lower the common mode rejection ratio (CMRR) of the biopotential amplifier during the measurement of the impedance. This lowers the coupling of the motion artefacts and power-line interference.

In addition to the contact pressure variations, also external pressure applied to the interface between the skin and the electrode will cause artefacts to appear in the measurement results. The artefacts have been suggested by Thakor and Webster in [120] to be caused by the different metabolic activity levels in the skin layers (stratum corneum, dead cells and inner layers, viable cells). The generator of the artefact potential has been proposed to lie in the stratum granolosum and the pressure changes will change the metabolic activity of the layers thus causing a potential difference between the inner and outer layers of the skin.

Ödman studied the temperature dependency of the potential differences between different skin layers as well as the effect of electrode radius of curvature into the artefact amplitude

[137]. In the research, he observed that the increasing temperature will lower the artefact potential and with increasing radius of curvature of the electrodes, the artefact potentials were also reduced. The original assumption of Thakor and Webster was that the artefact current remains constant as the skin is being compressed [120]. Talhouet *et al.* further investigated the artefacts related to the skin deformations by stretching the skin and they observed both rapid and slow variations in the potentials of the skin layers. Rapid variations are mostly due to the resistance change in the signal route between the deeper and surface skin layers but the slow variations were assumed to be due to the artefact current changes. [17]

Filtering the measurement signal can also reduce the artefacts in it. Filtering is, however, problematic since the frequencies where the artefacts lie, often overlap with those of the measurement signal. Therefore filtering of the measurement signal also rules out a part of the information contained by the signal. [28] Barros *et al.* have suggested in [5] to utilise higher order signal conditioning methods to remove the overlapping noise from the original signal. They utilised independent component analysis (ICA) in the signal conditioning and were able to separate the artefact signals effectively from the original measurement data although they overlapped in the frequency domain.

In addition to movement artefacts in the measurement signal that originate from the movement of the electrode with respect the skin or skin layers, there may exist another movement induced artefact signal. The artefact is caused by the static charge accumulated to the body of the measurement subject or in the body of somebody else in the vicinity of the subject. The moving charges cause artefacts in the measurement signal. The artefact type is called triboelectric interference due to its birth mechanism. [34]

The electrodes suffer also from electrochemical noise originating from impurities adsorbed by the electrodes. Aronson and Geddes have investigated the effect in [2] and found that a pair of electrochemically clean electrodes are very stable. However, after introducing a minute amount of impurity on one of the electrodes, the electrochemical noise exhibited by the electrode pair is greatly higher. The noise is due to the unstable current that will flow in the electrode surface layer due to the short-circuited cell of two dissimilar metals of the electrode and the contaminant. [28]

The biosignal quality and motion artefacts can also be enhanced by preconditioning the skin under the electrode. [28] Talhouet *et al.* made measurements on the relationship between skin rubbing and electrode–skin interfacial impedance. [17] According to their measurement results, the impedance between the electrodes and skin reduces when the skin has been rubbed with a tape or a piece of sandpaper. Lower absolute impedance values at the interface also induce lower variations which means smaller motion artefacts. Proper selection of the electrode material and skin preparation may also reduce slow baseline drift observed in the surface electrode measurements [29].

The artefacts in the bioelectrical signals are not always only an undesirable property. Pawar *et*

al. have found in [93] that the artefacts in the measurement signals can be used to determine various body movement activities. They were able to categorise even very subtle movements of test persons with relatively good accuracy. They used principal component analysis (PCA) in determining the most probable movement that has caused observed artefact in the measurement signal.

2.7 Electrode-electrolyte interface noise measurements

The knowledge of the electrochemical noise arising from the electrode–electrolyte interface is essential in determining the most suitable electrode material or setup to be used in the current application. The electrochemical noise of a virtually still interface can reach noise voltage values as high as tens of microvolts up to tens of millivolts [28]. The biopotentials to be measured with the electrodes may be only few tens of microvolts in amplitude e.g. in EEG so the intrinsic noise in the electrodes may introduce truly remarkable problems.

The electrode immersed in an electrolyte is always in floating potential and therefore another electrode, called the reference electrode, is needed to set the potential of the electrolyte at some fixed level to which all other potentials are referenced. [14, 28] Hence, the measurement of the electrochemical noise of the interface has to be performed with two electrodes. To obtain the actual electrochemical noise of some electrode–electrolyte pair, one has to have a reference electrode whose properties do not interfere with the measurement. Reference electrodes are shortly discussed in section 2.3. A hydrogen electrode is a good reference electrode to be used as a stable counterpart for the electrode under investigation. This method can be, however, time consuming and complex to apply.

The measurement method typically used for the measurement the electrode–electrolyte interface noise is rather straightforward. Aronson and Geddes suggested in [2, 28] that one takes two identical samples of the electrode material under test and immerse these in the desired electrolyte. Then the electrodes are connected to a high impedance differential measurement amplifier and the differential voltage signal is measured. The resulting electrochemical noise is not directly the noise of the electrode–electrolyte interface but it is the voltage noise between the two electrodes. In relation to real-life measurements, this is typically the noise which is interesting and has practical importance and whose amplitude should be minimised.

Huigen *et al.* have conducted a research about the electrochemical noise at the interface [43]. The measurements clearly indicate that the electrochemical noise is a strong function of stabilisation time that the electrode and the electrolyte are let to be in contact with each other. The research suggests that all materials will reach the same noise level after they have been stabilised with the electrolyte. Some materials show more rapid stabilisation times than others. This leads to time dependency in all electrochemical measurements.

Due to the time dependency of the electrochemical noise the electrode exhibits, the electrochemical noise should either be measured as a function of time or the time the electrode–electrolyte interface is let to stabilise. The time of stabilisation should be determined so that it corresponds to the real-life measurement situation. The interface stabilisation times with the most practical importance are short since the noise measurement then best corresponds to a situation where e.g. motion artefacts are present. After an artefact, the stabilisation process of the electrode–electrolyte interface starts all over again. However, in measurement applications, the measurement of the biosignal continues immediately after the artefact whether the electrode has been stabilised or not. This means that the time of stabilisation remains short.

Several stabilisation times for the interfaces have been used in different studies. Huigen *et al.* in [43] used immediate measurements of the interface noise up to several hours of stabilisation time for face-to-face mounted standard pre-gelled electrodes. McAdams *et al.* on the other hand used stabilisation time of five minutes for gold (Au) electrodes in phosphate buffered saline (PBS) solution [68]. Aronson *et al.* used an immediate measurement of the electrochemical noise of the electrodes [2]. Typical electrode stabilisation time is measured in minutes, usually only few minutes of stabilisation is enough to produce low electrochemical noise in the measurements.

Harland *et al.* have presented a contactless (capacitive, only displacement current involved) biopotential measurement which by its nature does not have a stabilisation time [37]. However, Casas *et al.* have studied the limitations and inaccuracies related to the capacitive measurement method and reported it not being as reliable as direct contact measurements [11].

The measurement of the amplified electrochemical noise can be made with a data acquisition card (DAQ) or it can be measured using a spectrum analyser. When a DAQ is being used, the measurement will be made in the time domain whereas with the spectrum analyser, the measurement results will lie in the frequency domain. Whichever method is used in the measurement of the voltage noise, the outputs of the measurements of different materials with small variations are not easy to compare with each other. Therefore typically a root-mean-square (RMS) noise will be calculated from the results. The RMS noise values are easier to be compared with each other.

When the measurement of the electrochemical noise between two identical electrodes is performed by using a spectrum analyser, the output of the measurement is the voltage spectrum of the measurement. Also, if the measurement was originally made with a DAQ, the measurement results can be converted from the time domain into the frequency domain with the fast Fourier-transform (FFT) and the similar frequency spectrum will be obtained [8]. Conversion from the time domain into the frequency domain enables one to calculate the RMS noise value on a specific frequency interval. This is essential since the biopotential measurements are performed on a limited frequency interval and the noise originating at frequencies outside of this interval is not relevant, in fact inclusion of it in the RMS noise value is misleading.

The RMS noise can be calculated from the discrete voltage density spectrum as

$$v_{\mathrm{rms}}^{\mathrm{f}} = \sqrt{\sum_{i}^{N} v_{i,\mathrm{f}}^2 \cdot \Delta f} \tag{2.5}$$

where N is the serial number of the highest discrete frequency component to be included into the calculations and $v_{i,\mathrm{f}}$ is the value of the i:th sample in the voltage density spectrum whose unit is $\mathrm{V}/\sqrt{\mathrm{Hz}}$ and Δf is the frequency step. For the case, where the voltage spectrum has been calculated by the FFT, $N = N_{\mathrm{fft}}/2$ where N_{fft} is the length of the FFT. The noise measurements presented in publications P2 and P7 were done with a spectrum analyser and in P6 with a DAQ card.

2.8 Impedance measurements of the electrode-electrolyte interface

The impedance of the electrode–electrolyte interface affect the biosignal to be measured. High impedance in this interface will also provide the external disturbing signals with a high impedance route to couple to the measurement electronics. The problem is even greater if the disturbances are not coupled as common mode signals. In this case, the CMRR of the measurement amplifier does not help in reducing the noise. The disturbances are not coupled as common mode signals when the electrode–electrolyte interfaces are not similar between the measurement electrodes. The problem has been researched by Huhta *et al.* in [42] who studied the power line interference coupling to the electrodes and leads. To avoid using electrode materials with the highest impedance, the knowledge about the interface impedance is important.

The values of the interface components shown in Fig 2.3(d) are typically given as the total impedance and phase of the interface or real and imaginary parts of the total measured impedance. Earlier, the measurement of the resistive and reactive parts separately was not regarded so important and only the total impedance was measured. Grimnes *et al.* have published a paper about two measurement setups that are able to measure individual electrode–skin interface impedance [35]. Possibly the earliest measurement method was suggested by Horton *et al.* in 1935 using two electrodes and a reference electrode [41].

When the impedance and phase are plotted against frequency, the resulting graph is called a Bode-plot and when the real part of the impedance is plotted against the imaginary part of the impedance, the plot is called a Nyquist-plot. Characterisation of the electrode interfaces is reported in this way e.g. in [6, 68, 70, 78].

More sophisticated way of characterising the interface is to report the values of the single components inside the interface electrical equivalent model. The measurement method to measure the independent component values depends a little on the used interface model. If the series connected resistor–capacitor model illustrated in Fig 2.4(b) is used, Nihtianov *et*

al. have in [82] presented a simple and low cost method to determine the resistance and capacitance values from the measurement data. The measurement method is based on an oscillating circuit where from the time delay between the measured voltage values the interface component values can be calculated.

In case of more complicated circuit models e.g. Fig 2.3, the measurement of the component values can be measured by utilising electrochemical impedance spectroscopy (EIS) [27, 98]. Usage of the EIS method demands special instruments and conditions so that the measurements can be done. The method applies a sinusoidal voltage or current between the electrode under study and the counter electrode whose properties are known. The measurement results are then fitted numerically to match the component values of an interface model such as in Fig 2.3(d). The applied frequency of the sinusoidal input signal can be varied which enable measurements of the component values against frequency. EIS is typically used in corrosion detection or measurements related to corrosion in general [100].

In addition to the EIS method and apparatus, less complex measurement methods to determine the interface component values do exist. One method presented by Lario-García *et al.* in 2003, was utilising two sinusoidal waves that were phase shifted with respect to each other by 90°. Applying these waves into the electrodes, three independent components could be calculated with 1.3 % accuracy [60].

Another method presented again by Lario-García *et al.* used square waves in the stimulation of the interface and it was originally implemented to determine the conductivity of an electrolytic solution [58]. A further application of the method to contain a constant phase element (CPE) was presented by Lario-García *et al.* in [59]. The author applied the method to determine the interface component values of the electrode–electrolyte interface when the conductivity of the electrolyte and its geometrical dimensions are known. These measurement setups and measurement results are originally discussed in P1 and P6 and revised in Section 3.3.2.

The measurement method suggested by Lario-García *et al.* and applied by the author, assumes a two-electrode system to be stimulated with a square wave waveform at frequency f. Duty cycle of the square waves is constantly kept at 50 %. The analysis is based on the equivalent circuit model shown in Fig 2.4(a) enhanced with the bulk resistance resulting in the Randles circuit equivalent model [97]. A schematic figure of the measurement situation of the interface impedance components with the proposed square wave method is presented in Fig 2.6. The interface component names are as in Fig 2.3(d) and Fig 2.4(a), V_S is the square wave voltage source amplitude, R_x denotes the resistance of the electrolyte and R_{meas} the measurement resistor resistance.

When the square waves are applied between the electrodes, the capacitance of the interface will modulate the square waves according to Fig 2.7. A measurement resistor is connected in series with the signal path and the voltage response is measured. From the response,

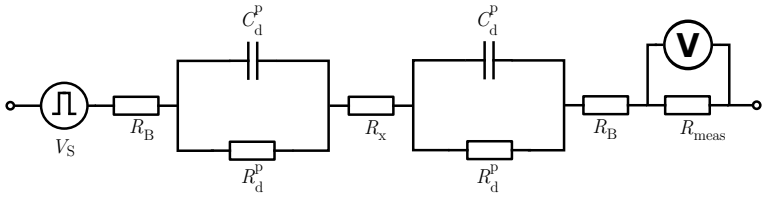

Fig. 2.6. *Schematic figure of the interface impedance measurement situation with the square wave method.*

the voltages of three separate time stamps are read. The time stamps can be chosen freely between 0 and T, the half period of the applied square wave, but the earlier time instants are favoured since they have a higher SNR and contain more information about the interface than the points at the end of the square wave half period. The interface electrical equivalent circuit values R_{B}, $R_{\mathrm{d}}^{\mathrm{p}}$ and $C_{\mathrm{d}}^{\mathrm{p}}$ can be calculated from the measured values. The model assumes both the electrodes to have identical interfaces.

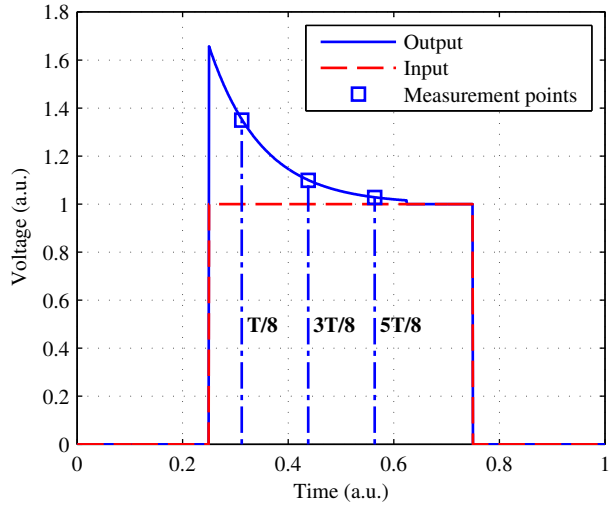

Fig. 2.7. *Stimulating square wave, modified wave by the electrode–electrolyte interface and voltage measurement points. T is the half period of the square wave. Picture originally presented in P6.*

Although the stimulation of the electrode network is done with square waves that include all possible frequencies, it is still possible to obtain the values of the interface impedance as a function of frequency. The frequency f at which the square waves are exitated will reflect the frequency behaviour of the electrode interface components at the same frequency. This is reported in P1 and P6 for the interface components and for the electrolyte resistance in [58].

When the suggested measurement method is used, the resistance of the electrolyte between the electrodes must be known. The resistance of the electrolyte between the electrodes is not

obvious if the electrodes are smaller in size than the electrolyte cross sectional area. In this case, the current between the electrodes will flow in the volume between the electrodes and not limit itself strictly in the cross sectional area of the electrodes. Therefore the resistance of the electrolyte is lower than in the case where the electrolyte volume would be exactly the same size with the electrodes. The resistance is called the electrolyte spreading resistance [54].

The electrolyte spreading resistance can be defined by finite element method (FEM) modelling when the conductivity of the electrolyte is known. FEM modelling can be used to simulate the current density between the two electrodes. With the FEM program, the user defines the voltage to be applied between the electrodes. By integrating the resulting current density over the surface of one of the electrodes, the total current flowing between the electrodes can be determined. By applying the Ohm's law, the resistance of the electrolyte can be obtained. The proposed method has been used in P1. There are, however, equations to calculate the electrolyte spreading resistance analytically. Equations are presented for e.g. in [54], but they are limited to only either square or circular electrodes.

In some cases, e.g. in case of P6, the electrodes are prepared to match, or exceed, the size of the electrolyte between the electrodes which simplifies the determination of the spreading resistance: Due to the lack of edge effects at the electrodes, the current density will be constant throughout the electrode area that contacts the electrolyte. This demands, however, that the pressure on the electrodes is sufficient to keep them in steady contact with the electrolyte. Furthermore, when the electrodes are sufficiently far apart from each other, i.e. several millimetres, the capacitive coupling between the electrode parts exceeding the electrolyte area is negligible and the whole electric field between the electrodes will be confined to the volume of the electrolyte.

In cases, where the volume of the electric field between the electrodes is well defined, the volume resistance of the electrolyte can be calculated by using the simple formula for resistance:

$$R_{\mathrm{x}} = \rho \frac{l}{A_{\mathrm{e}}} \tag{2.6}$$

where ρ is the resistivity of the electrolyte, l is the separation between the electrodes and A_{e} the confronting area of the electrodes.

The measurements are performed with a signal generator that is able to produce square waves and a DAQ. Voltage measurements at three time stamps are needed for the determination of the impedance components. The time stamps shown in Fig 2.7 were suggested by Lario-García *et al.* in [58] and the same time stamps were adopted to the research of the author as well. The equations to determine the interface electrical component values are somewhat modified from those of Lario-García's. The derivation of the equations was based on Fig 2.6 whereas in [58], the model was slightly compressed and the derivation of the equations was based on that model.

The calculation of the independent component values demands some additional variables to be defined:

$$\Delta T = \frac{T}{8} \tag{2.7}$$

$$I_S = \sqrt{\frac{I_U(3\Delta T) - I_U(\Delta T)}{I_U(5\Delta T) - I_U(3\Delta T)}} \tag{2.8}$$

$$\alpha = \frac{\ln|I_S|}{\Delta T} \tag{2.9}$$

$$A_T = \frac{(I_U(3\Delta T) - I_U(\Delta T))(1+\exp(T\alpha))}{2[\exp(-3\Delta T\alpha)I_U(\Delta T) - \exp(-\Delta T\alpha)I_U(3\Delta T)]\exp(T\alpha)} \tag{2.10}$$

$$I_F = \frac{I_U(3\Delta T)}{2A_T\exp(-3\Delta T\alpha)\frac{\exp(T\alpha)}{1+\exp(T\alpha)} + 1} \tag{2.11}$$

T is the half period of the applied square wave and I_U is the calculated current value from the voltage measurement result over the measurement resistor R_{meas}. The component values can be now calculated by using Equations 2.7–2.11:

$$R_{\text{B}} = \frac{V_0 - I_F R_{\text{S}}(1+A_T)}{2I_F(1+A_T)} \tag{2.12}$$

$$R_{\text{d}}^{\text{p}} = \frac{1}{2}A_T(R_{\text{S}} + 2R_{\text{B}}) \tag{2.13}$$

$$C_{\text{d}}^{\text{p}} = \frac{R_{\text{S}} + 2(R_{\text{B}} + R_{\text{d}}^{\text{p}})}{R_{\text{S}} + 2R_{\text{B}}}\frac{\Delta T}{\ln|I_S|} \tag{2.14}$$

where $R_{\text{S}} = R_{\text{x}} + R_{\text{meas}}$ is applied for clarity.

The derived equations 2.7–2.14 were verified with a circuit model in Fig 2.6 that was both modelled with a PSpice circuit modelling program and with a physical circuit model constructed of components with the same component values. The values of the components in the network as well as the induced square wave frequency were set to match the values used in the study by Lario-García *et al.* [58]. Table 2.1 summarises the results of the simulations and circuit board model tests. Both the electrode–electrolyte interfaces were constructed of components with similar values for clarity. The electrolyte resistance was set to be $R_{\text{x}} = 560\ \Omega$ and the measurement resistor $R_{\text{meas}} = 2.696\ \text{k}\Omega$. Frequency used in the stimulation of the square waves was 350 Hz and the sampling rate of the DAQ was set at 100 kHz to obtain accurate waveforms from the measurements. From Table 2.1 it can be seen that with sufficiently high sampling frequency of the waveform, the independent component values of the interface can be relatively accurately defined although the accuracy of the analysis was poorer than the one reported by Lario-García *et al.* in [58]. Noteworthy still is, that the measurements done with the constructed physical model indicate that the analysis done with the equations sug-

Table 2.1. *Values of the components used in the simulation and circuit model accompanied with the results of analysis based on the square–wave method. Errors of the calculations are given in percents inside the parentheses.*

Component	True value	PSpice simulation	Physical model	
			Author	Lario-García
R_B	389 Ω	386 Ω (0.87 %)	404 Ω (3.8 %)	419 Ω (7.7 %)
R_d^p	999 Ω	1002 Ω (0.40 %)	1092 Ω (9.4 %)	1131 Ω (13 %)
C_d^p	0.964 μF	0.964 μF (0.02 %)	0.998μF (3.5 %)	1.006 μF (4.4 %)

gested by Lario-García is slightly less accurate than the analysis done with newly defined equations 2.7–2.14.

3. PHYSIOLOGICAL SURFACE MEASUREMENT DEVICES USING ELECTRODES

3.1 A short introduction to biopotential amplifiers

The biopotentials that are measured are inherently low in amplitude. The ECG signals range from 0.1 up to 10 mV, EEG signals remain in the range of 10–100 μV measured from the skin surface [80, 132]. The signals have to be amplified in order to be able to record the signals for instance with a DAQ card. The amplifier, however, introduces additional noise to the measurement and the properties of the amplifier has to meet certain demands in order to be able to record the signals reliably.

In the biopotential measurements, the difference in the potential between two electrodes is measured. The resulting signal is called the corresponding biopotential and it is measured using a differential amplifier with voltage gain A, see Fig 3.1 [28, 105]. The amplifier–electrode

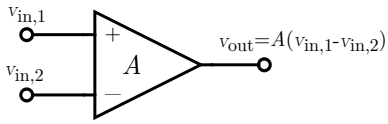

Fig. 3.1. *Schematic figure of the differential amplifier used to measure biopotentials.*

interface can be illustrated as in Fig 3.2. The amplifier includes current and voltage noise of

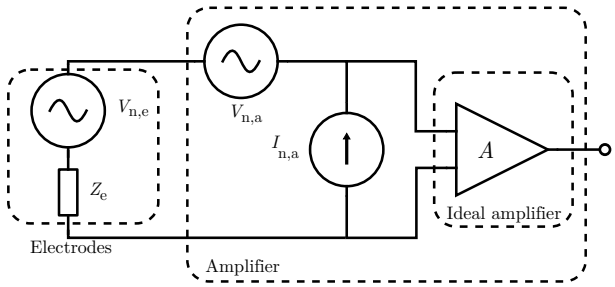

Fig. 3.2. *Schematic figure of the electrode–amplifier setup including the noise components that contribute to the measurements. Figure modified from [26, 33].*

its own that will contribute to the measurement results. This non-ideal behaviour is visualised

in Fig 3.2 with the dashed lines around the ideal amplifier and the real amplifier. Inside the amplifier, there are the voltage noise, $V_{n,a}$, and the current noise, $I_{n,a}$, of the amplifier. The electrode is also illustrated as having an AC noise source, $V_{n,e}$, which represents the combination of the electrochemical fluctuation of the electrode potential at the electrode–electrolyte interface discussed in detail in Section 2.6, and the thermal noise of the electrode impedance accompanied with the measurement resistance (the resistance of the wires). [26, 33] The total equivalent noise of the amplifier–electrode circuit will be [76]

$$V_{n,T} = \sqrt{V_{n,e}^2 + V_{n,a}^2 + I_{n,a}^2 Z_e^2 + 2CV_{n,a}I_{n,a}Z_e} \tag{3.15}$$

where C is the correlation coefficient between the amplifier voltage and current noise. All of the noise components can be, and most likely are, frequency dependent.

The measurement amplifier has a finite input impedance. The input impedance of the measurement devices has evolved significantly from the first decades of the 20th century when string galvanometers were being used to measure the ECG. The input impedance in these was as low as 5–20 kΩ [28]. Even in the 1960's, the input impedance of the biopotential amplifiers was not typically higher than a few megaohms [31]. The evolution of silicon technology has provided not only small sized components but also higher input impedance in the amplifiers. Nowadays, the amplifiers designed to measure biopotentials are typically instrumentation amplifiers, buffered differential amplifiers, constructed of three operational amplifiers owing an input impedance around for example 100 GΩ in parallel with 3 pF [118]. On the information band of the ECG signal, as presented in Section 2.4, the input impedance of the modern amplifier varies between 1.3–51 GΩ.

High input impedance in the measurement amplifier is essential in retaining the characteristics of the signal. When the input impedance of the measurement amplifier is high, the current drawn by the circuitry shown in Fig 3.2 remains low. This implies that the voltage drop across the electrode–electrolyte interface is small and the signal is recorded with almost the same amplitude as originally possessed at the electrode [28].

The noise components of the amplifier in Fig 3.2 are typically low and in majority of cases negligible. The spectral noise densities for INA333 instrumentation amplifier manufactured by Texas Instruments [118], measured at f=10 Hz, are $i_n = 100\ \mathrm{fA}/\sqrt{\mathrm{Hz}}$ and $v_n = 50\ \mathrm{nV}/\sqrt{\mathrm{Hz}}$. The total noise voltage of the amplifier at the information band of the ECG signal, see Section 2.4, can be estimated with the current and voltage noise density values at 10 Hz to be 0.3 $\mu\mathrm{V_{rms}}$. From Section 2.3 it can be read that for most stable electrodes, the reference electrodes, the voltage fluctuation can be at the lowest in the order of micro-volts. All other electrodes are lying well above these values, Section 2.7, so the noise of the instrumentation amplifier is not an issue.

The differential amplifiers are designed in such a way that the differential signals are amplified but common mode signals are not. The ability of the amplifier to reject the common mode

signals from being amplified is called the common mode rejection ratio (CMRR). CMRR is defined in dB scale as [42, 105]

$$\mathrm{CMRR} = 20\lg\left|\frac{A_\mathrm{d}}{A_\mathrm{cm}}\right| \tag{3.16}$$

where A_d is the differential gain of the amplifier and A_cm is the common mode gain. A typical value for CMRR in the 1960's was 60 dB [42], today typical values range between 90–115 dB [118].

The CMRR of the amplifier is in any case finite and many sources of interference are usually present in the measurement environment. Huhta *et al.* have presented a list of the three coupling mechanisms of interferences to the measurement [42, 119]:

1. Magnetic fields (induced into leads, from power line, motors, transformers, etc.)
2. Electric fields (displacement currents induced into the body from power lines, fluorescent lamps, etc.)
3. Electromagnetic fields (modulated RF signals, from diathermy, electrosurgery, etc.).

All the interference sources may cause substantial disturbances in the measurements. Magnetic disturbances can be rejected by keeping the area of the closed measurement loop small since the noise voltage the magnetic flux will generate in the measurement leads is proportional to the area. [42, 132]

The AC signals propagating in the power lines will be coupled to the measurement capacitively either through the person or the subject to be measured or through the measurement wires. The noise coupled to the measurement signal through the measurement leads between the electrodes and the first stage amplifier can be reduced by shielding the cables. [42, 73] The shielding of the cables can be carried out by using coaxial measurement leads with the shield connected into the ground potential of the measurement electronics [132].

The common mode potential coupled to the measurements through the patient can be reduced by feeding the common mode signal back to the patient using a so called driven right leg circuit. This is realised by using an amplifier that has a current limiter and feeds the signal to the patient through a third electrode [42, 73, 131]. The amplifier traditionally used has been an operational amplifier but Spinelli *et al.* have proposed to use a transconductance amplifier for this purpose. The usage of the transconductance amplifier allows wider bandwidth of the common mode signal and being a current feeding method, the electrode–electrolyte interface properties play no role in the compensation efficiency [109].

Metting van Rijn *et al.* have listed the properties of a good biopotential amplifier:

1. very high common-mode input impedance (> 100 MΩ at 50 Hz)

2. high differential-mode input impedance (>10MΩ at 50 Hz)
3. equal common-mode input impedance for all inputs
4. high common mode rejection ratio (> 80 dB at 50 Hz)
5. shielded input cables; the shields must be driven by a proper guarding circuit
6. additional reduction of common-mode voltage with a driven right leg circuit.

One further option to reduce the common mode interference from being coupled to the measurements is the usage of active electrodes [12]. The active electrodes will sense the potential as traditional, passive, ones but in addition they have the ability to amplify the signal at the electrode. This is realised by constructing the amplifier electronics either to the immediate vicinity of the electrode or the amplifier circuitry is constructed directly on the back side of the electrode [74, 83]. The usage of the active electrodes has been proved to be a very effective means to reduce the common mode interference in the measurement [12, 74]. Nishimura *et al.* showed that the use of an active electrode reduces or completely removes the need for preparation of the patient skin prior to the measurements. They were also able to leave out the conductive electrolytic gel from the interface and still gain good quality measurement results. [83]

3.2 A selection of surface measurement devices measuring ECG and bioimpedance

To get an overview of some of the surface measurement applications where electrodes and especially textile based electrodes are being used, a very brief and compact literature review on the subject is presented.

Vuorela *et al.* have presented portable, lightweight measurement devices to measure bioimpedance [127, 128]. The devices are designed for measuring the ECG and respiratory parameters of a human by means of bioimpedance measurement and data analysis. Seppä *et al.* have successfully used the devices in measuring ECG and ventilation parameters non-invasively from test persons with minimal body geometry deformations due to physical activity [106]. They have also measured the minute ventilation of a running test person with the device with relatively good success [107].

The bioimpedance measurements have also been used in the determination of the water balance of humans. Medrano *et al.* have presented in [69] a portable bioimpedance measurement system to determine the water balance in humans. Medrano *et al.* have further measured the water balance from elderly people as a part of treatment in nursing homes [71].

The determination of the minute ventilation with the aid of bioimpedance measurements is a time domain measurement where the frequency of the system is kept constant. In applications reported by Seppä *et al.* in [106–108], the applied frequency was around 100 kHz. In applications for determining the water balance, the approach to the problem lies in the frequency plane. The frequency of the signal drawn between electrodes is swept and the response of the measured impedance plotted. The water balance can be determined from the impedance by utilising the Cole-Cole model [66, 69]. The frequencies used in the research by Medrano *et al.* varied between 5 kHz and 1 MHz. In general, the bioimpedance measurements can be used to obtain information on a very large scale of illnesses and function of the organs. A good list, yet not necessarily complete, of possible measurement targets is given in [123].

In an article presented by Mühlsteff *et al.* [79], they suggested a portable and wearable measurement device capable of measuring the ECG of the test person as well as his activity. The device incorporates electrodes constructed of carbon-loaded rubber moulded in a form of a band that is to be placed around the thorax of the test person. The results achieved with the rubber electrodes were fairly good. However, the initial settling of the electrodes to reach a stable level took 3–15 minutes depending on the person and the skin properties. 5–10 seconds of data was typically lost when motion artefacts were introduced.

Rita Paradiso with her research group has been very active in the field of wearable measurement applications employing textile electrodes [62, 89, 91]. They have been researching textile yarns to be used as conductors in smart clothing and the use of textile electrodes to measure mainly ECG. In an article by Paradiso *et al.* [91] there is a presentation of a wearable, comprehensive health monitoring system which uses knitted textile electrodes to measure ECG. The electrodes have been made of a thin stainless steel wire. To improve the electrical signal quality under dynamic conditions, a hydro-gel membrane was being used with the electrodes. Based on the data and figures presented in [91], Paradiso has also applied for a US patent for the method of measuring respiratory, movement and cardiac signals with knitted electrodes arranged in a certain way on the garment [88]. The same hydro-gel membrane was used in a paper by Puurtinen *et al.* where the textile electrode behaviour was examined when placed on human thigh both dry, wet and with hydro-gel membrane [95]. The results indicate that the hydro-gel enhanced interface between skin and electrode shows higher stability than dry or even wet electrode.

Nowadays, the market potential for portable, light-weight physiological measurement devices to measure ECG or heart rate is huge. There are several commercial applications on the market that measure the heart rate of a test person. The technique of measuring the ECG and deriving the heart rate from the ECG signal is well-known and easily accessible by everyone. Therefore the accuracy of the devices and overall quality are widespread. The majority of the measurement devices rely on carbon loaded rubber electrodes attached on a belt that is mounted around the chest of the test person. Two major Finnish players in the heart rate mon-

itor markets are Suunto (http://www.suunto.com) and Polar (http://www.polar.fi/en). Suunto has collaborated with a Finnish software house, Firstbeat (http://www.firstbeat.fi), regarding the R-spike identification algorithm. The two presented companies are also respected internationally although there are companies like EKHO (http://www.ekho.us) and Timex (http://www.timex.com) that are more incorporated in the US markets. Although the technology used in the electrodes of these commercial devices has been proved to be feasible, still it is not suitable for continuous long-term monitoring due e.g. to the discomfort the electrode belt causes to the subject. Hence, more research is needed before electrodes suitable for the mass market and capable of performing long-term measurements can be assumed to appear on the market.

3.3 Surface electrode characterisation results

The interface noise originating from the electrode–electrolyte interface is one of the crucial components to be aware of when choosing electrode materials for surface measurement applications. Section 2.6 introduced various mechanisms that give rise to artefacts that disturb the measurements. One of the artefacts is the interface noise whose measurement principle has been introduced in Section 2.7.

In surface measurements, relatively short stabilisation time for the electrode–electrolyte interface is desired. Typically Ag/AgCl -electrodes are used which are generally known to possess suitable characteristics to be used in the sensitive surface bio-potential measurements often suffering from artefacts [43]. Other metallic materials to be used as bio-potential electrodes were also researched under the conduction of the thesis to find out their performance with respect to Ag/AgCl electrodes.

The size of the measurement electrodes should be in relation with the electrochemical noise it exhibits and the interface component values should change as a function of the size. These issues were also studied with measurements. Theoretical calculations for the noise–area relationship are presented in an article by Huigen *et al.* [43]. P2 reports the electrochemical noise of electrodes made of the same material but having different sizes. P1 and P7 report the relationship between the electrode–electrolyte interface component values with respect to the changes in the geometrical area of the electrodes.

3.3.1 Results of electrode-electrolyte interface noise measurements

Several noise measurements were conducted first of which was made with Ag, Ag/AgCl and Pt electrodes (P7) and the second with Ag, Au, Pt and stainless steel electrodes (P2) immersed in a liquid electrolyte. The research reported in P2 also the effect of the electrolyte having on the measured noise was studied. Three electrolytes were used: saline (0.9 m-% NaCl),

phosphate buffered saline (PBS) and simulated body fluid (SBF). The size of the Ag and Ag/AgCl -electrodes was varied by a factor of two in the first experiment (P7). The second experiment (P2) with four electrode materials also included electrodes in two different sizes where the sizes for all electrode materials were varied by a factor of two.

The noise measurements were performed in the first experiment with an Agilent spectrum analyser 4396B and in the second experiment a spectrum analyser HP3561A by Hewlett-Packard was used. The results were mean valued over 16 or 32 samples to reduce the variance in the results [4].

The noise measurements done and reported in P7 clearly show that with relatively short stabilisation time of two minutes, the Ag/AgCl electrodes exhibit the least electrochemical noise thus they are very suitable for surface measurements where both movement artefacts are present (sport applications or medical applications including possibility of movements) and/or the measurement results are needed rapidly after applying the electrodes on the skin of the subject (e.g. hospital environment, emergency care in an ambulance).

Measurement results reported in P2 reveal the differences in the electrochemical noise measurements between three electrolytes. The electrolytes had different conductivities which were measured with a four-wire conductivity meter. The conductivity of saline was measured to have a conductivity falling in between the two other electrolytes, PBS and SBF. According to the measurement results, the steel electrodes (material AISI 316L) showed low electrochemical noise levels after being stabilised for one minute. They exhibited even lower noise levels than the Ag/AgCl electrodes which are generally regarded as the electrodes exhibiting the lowest noise level [43], P7. Au electrodes were measured to be the third best alternative as electrode material with respect to low electrochemical noise. Pt electrodes showed the highest noise level after the stabilisation time of one minute.

The relation between the surface area and the electrochemical noise the electrodes exhibit, obey the theory presented in [43] relatively good in the previously mentioned publications. The electrochemical noise amplitude should be inversely proportional to the square root of the electrode area. The relation between the measured electrochemical noise and the area of Ag/AgCl electrodes does not match the theory in P2. The problem is most probably due to imperfect AgCl-layer on the Ag electrode. The chloriding process was taking place in a saline solution with a 3 V potential difference with negative polarisation between the working and target electrode and the process was held on for two minutes. Longer time would have provided a more stable AgCl layer [113, 130]. Despite imperfect AgCl layer on the Ag electrode, it is obvious that the AgCl coating has a stabilising effect on the electrochemical noise behaviour of the Ag electrodes.

For wearable applications, the textile electrodes are a more feasible choice for electrodes than purely metallic ones researched in the previously mentioned studies. Electrochemical

noise measurements were also done with textile electrodes. The measurements and results are reported in P6.

In the noise measurements of the textile electrodes, four different textile electrodes were used. The conductive material in the electrodes was either silver or copper coated polyamide fibre. One of the electrodes also had a conductive polyuretane layer on the reverse side of the electrode. Silver has been widely used in textile electrodes [6, 16] although fibres made of stainless steel have also been used [89]. The electrolyte used in the measurements was made of Agar-gel and for the measurements it was cut to a block of size (l,w,h) 5.3 x 5.1 x 4.7 cm. The conductivity of the Agar-block was set to match the conductivity of a wet human skin. The electrodes to be measured were applied on top and bottom of the gel block. A special measurement stand and setup was used to apply a constant static pressure on the electrodes to secure a good galvanic contact between the gel and the electrodes. The measurement stand has been presented by Beckmann *et al.* in [6]. The electrodes were cut from the fabric so that they had area slightly exceeding that of the Agar-block's. The excess area was used to connect the measurement wires to the electrodes by crocodile clips as well it defined the orthogonal contact area of the electrodes to be exactly the same as the size of the Agar-block thus all measurements are equivalent in electrode area since the same block was used throughout the measurements.

An instrumentation amplifier AD620BRZ by Analog Devices was used to sense and amplify the differential signal from the electrodes. The amplified signal was measured with a National Instruments USB-connected DAQ, type USB-6251 BNC. The signal was then converted from the time domain into the frequency domain by applying an FFT-algorithm on the data. The RMS-noise of the electrode was calculated using Equation 2.5 and bandwidth which was used was lying between 0 and 500 Hz.

The electrodes were applied on the Agar-block and the measurements of the noise were begun primarily after two minutes. The electrode noise data was recorded for 70 s each time and the measurements were performed after the initial measurement at 5, 10, 15, 20, 25, 30, 45 and 60 minutes from the application of the electrodes on the Agar-block. The time instants of the individual measurements serve as the time the electrode–electrolyte interface has been let to stabilise. The RMS-noise of each measurement section was calculated and the noise of different materials were compared as a function of time. In addition to use four different electrode materials, also three different preparation schemes were being applied on the electrodes: dry electrodes (unconditioned), electrodes with a hydrogel membrane supplied by ST&D Ltd., Belfast, U.K. at the interface to enhance the contact with the electrolyte and electrodes moistened with the PBS solution to mimic sweat on the skin.

The measurement results reported in P6 clearly indicate that despite the material of the electrode, the stabilisation time remains under 10 minutes. Only some materials showed longer stabilisation times, 25–30 minutes, when they were unconditioned or had a hydrogel mem-

brane between the electrode and the electrolyte. Results also indicated that the electrodes that had been moistened with the PBS, showed the most stable behaviour with time. All the four tested materials seemed to have been stabilised after 10 minutes of application. The ratio of the electrochemical RMS-noise between measurements done after 2-3 minutes the application and measurement after 10 minutes or more is one decade in almost any case. In fact, the noise value has been reduced by a decade between the measurements at 2-3 and 5 minutes yet the interface is not completely stabilised.

What was surprising in the results was that the RMS-noise values of all materials rose between 30 and 45 minutes. An explanation for this kind of behaviour could be that the interface dries up. This would especially be the case with hydrogel and PBS treated interfaces. The same behaviour was, however, seen for the unconditioned electrodes as well. Of all materials only for one material, called Kassel RS, the RMS value decreased again as time elapsed from 45 to 60 minutes. The material was the only material for which the conductive fibres were partly made of copper. Another possible explanation for the elevated noise values at 45 and 60 minutes is that the electrode textiles themselves absorb moisture from the Agar-block causing the interface to be in a state of constant variation.

3.3.2 Results of impedance measurements of the electrode-electrolyte interface

The impedance measurements of the electrode–electrolyte interface for the materials used in the research in P7 were performed with an LCR-meter HP4262A by Hewlett-Packard. The measurements were performed at two frequencies, 120 Hz and 1 kHz. The results obtained with the measurement device are, however, erroneous when compared to results reported in P1 or values e.g. in [28]. The resistive part of the interface impedance according to P7 is in the order of tens of ohms although according to results obtained in P1, the resistive part is in the order of hundreds of kilo ohms with virtually the same contact area. The results of the latter are in line with the results shown in [28]. Reason for the errors occurring in the measurement results is unknown yet with high probability errors are due to LCR-measurement device's capability to reliably measure impedance lying in this range. The results obtained in P7 seemed to satisfy the measurement scale of the device but when results in [28] or P1 are examined, the span of the measurement range is no longer enough to measure the interface components correctly.

Consecutive electrode impedance measurements were done with the measurement method utilising square waves. The method is discussed in more detail in Section 2.8. Measurements presented in P1 were done with Au, Pt, stainless steel (AISI 316L) and Ag/AgCl electrodes and they were performed at 40, 75, 110, 200 and 350 Hz. The input and output waveforms illustrated in Fig 2.7, were measured with a PCI-6052E DAQ by National Instruments. The measurement current density varied between 850 μA/cm^2 and 2000 μA/cm^2 depending on the separation and area of the electrodes. In the analysis of the measurement results, the modified

Warburg circuit equivalent was used, namely the low frequency approximation illustrated in Fig 2.4(a). This model was used because the analysis was found to be very sensitive to the accuracy of the measured waveforms and erroneous results, e.g. imaginary resistances, were obtained when the most complex circuit equivalent was used as shown in Fig 2.6.

Interface component measurements indicated that the Ag/AgCl electrode had the greatest interface capacitance compared to other materials under research. This seems to be in controversy with the known fact that Ag/AgCl is a non-polarised material whose behaviour at the interface should be mainly resistive. However, according to results obtained in P1, the interface resistance of Ag/AgCl is much lower than for other three materials. Capacitance is, however, greater but the same behaviour has been reported in [28] as well. In conclusion, the square wave measurement method of the interface component values seems to be applicable also in the case of non-polarised materials. This statement is opposite to what is stated in P1.

The power law behaviour of interface resistance and capacitance mentioned in Section 2.4 was verified in the research. The slope of interface resistance for polarised materials (Pt, Au and AISI 316L) was calculated to be between 0.70 and 0.95 for 7 x 7 x 0.5 mm electrodes and from 0.43 to 0.54 for 3.5 x 7 x 0.5 mm electrodes. The corresponding powers for interface capacitance were between 0.16 and 0.26 for electrodes with greater area and 0.34 and 0.48 for electrodes with smaller area. The values of the slope of the impedance vs. frequency plot are in good relation with the values suggested in [7, 14, 28, 30, 103, 126]. It is interesting to note that the slope of the exponential curve depends on the area of the electrode. It seems that the absolute value of the slope of the resistance as a function of frequency is proportional to the area of the electrode whereas the absolute value of the capacitance slope is inversely proportional to the area. For non-polarised electrodes, Ag/AgCl, the slopes were not calculated due to the partly non-linear behaviour of the impedance curves. The non-linear behaviour is most probably related to the current density at the electrodes.

Impedance measurements made with textile electrodes were conducted in the same manner as for the solid metallic electrodes revised earlier in this chapter. The measurement range was, however, only up to 10 Hz due to a very low signal level at higher frequencies. Impedance measurements were performed after the noise measurements without breaking the connection of the electrode and electrolyte. According to Mühlsteff *et al.* [78], the interface impedance has reached its long-term equilibrium after approximately 60 minutes. More specific explanation about the measurement setups and measurement results can be found in P6.

The slope of the resistance and capacitance vs. frequency that were obtained in the measurements were between 0.14 and 0.58 for resistance and 0.62 to 0.80 for the capacitance. The values for resistance vary a lot yet covering the whole range estimated by the models presented in Section 2.4. The values calculated for the capacitance were more constant than for the resistance and the variation was smaller both between the electrode materials and the electrode preparations. The measurement alternating current density was kept on a low level

being only 0.61 μA/cm^2 which guaranteed the impedance to lie in its linear range while the direct current density was 5 nA/cm^2. According to Bera *et al.* this kind of superimposed AC- and DC-stimulation more reliably simulate the actual measurement situation and more realistic measurement results are obtained [7]. From the measurement results the same tendency as for the RMS-noise could be seen: the preparation of the electrode–electrolyte surface gave more stable measurement results. The PBS conditioned interface gave the most stable measurement results.

The interface resistance of the textile electrodes with respect to their unit geometrical area was in the range of 3 kΩ/cm^2 whereas for the metallic electrodes it was in the order of 1 MΩ/cm^2. For the interface capacitance, the corresponding numbers were 4 μF/cm^2 and 180 μF/cm^2, respectively. Based on these measurement results, the textile electrodes seem to be more non-polarised than the solid metallic electrodes. On the other hand, the conductive material of the textile electrodes was also different, Ag or Cu, whereas for the metallic ones the interface material was one of the following: Ag, Ag/AgCl, Pt, AISI 316L or Au. Also the effective area of the textile electrodes is much larger than their geometric area. Therefore the values calculated for the components per unit area are not directly comparable.

4. IMPLANTABLE PHYSIOLOGICAL MEASUREMENT DEVICES

4.1 Devices for monitoring purposes

Monitoring and measuring the laboratory animals is a frequently used method in conducting scientific researches, e.g. drug experiments. As the laboratory animals are typically small, rats for example, implantable applications with wireless links to an external reader device are in many cases good alternatives for long term measurements thanks to their user friendly appearance for such purpose. Implantable devices also allow free movement of the animals without disturbing wires. In short term studies, the implanted devices are not necessarily the best choice to be used as physiology measurement devices because of the risks and inconvenience related to the implantation [86]. Implantable devices with wireless link to the external reader device are subject to regulations of the allowed radio frequency (RF) radiation in the subject body. Standard stating the limits for radiation still considered harmless to the body is the IEEE/ANSI c95.1 – 2005 standard [45]. In the development process of new measurement devices, the recommendations stated by the standard have to be taken into account. Although the recommendations are given with respect to human exposure of the RF radiation, the same values can be successfully applied to the animal applications as well.

Kramers *et al.* have reported of an experiment with an implantable blood pressure (BP) measurement device implanted in mice. Alternative way to measure the blood pressure of the laboratory mice has been the indirect tail-cuff plethysmography method (surface measurement). According to their research, the mice with the implantable devices exhibit lower stress levels than the mice whose blood pressure is being measured with the traditional tail-cuff method. The greatest individual factor contributing the stress level of the test animals is the implantation procedure. [56]

In the following sections, a brief review is being introduced regarding implantable applications used for measuring of biopotentials and blood pressure. Biopotential measurement is essentially related to the thesis and implantable devices measuring ECG have been discussed in P3, P4, P5, P8 and P9. The blood pressure devices are taken into account since many of these also enable measurement of biopotentials and blood pressure measurements have been performed with resonance-based measurement devices. A resonance-based measurement device is presented in P5 and therefore other resonance-based devices are in relevance

to the thesis. The implantable devices are divided into three groups: Battery powered devices, sometimes called active implants, inductively powered devices, also known as passive implantable devices and resonance-based devices, which are totally passive devices without any active electronic components. Fig 4.1 shows a block diagram of the three device groups together with the applications related to these groups presented in the text.

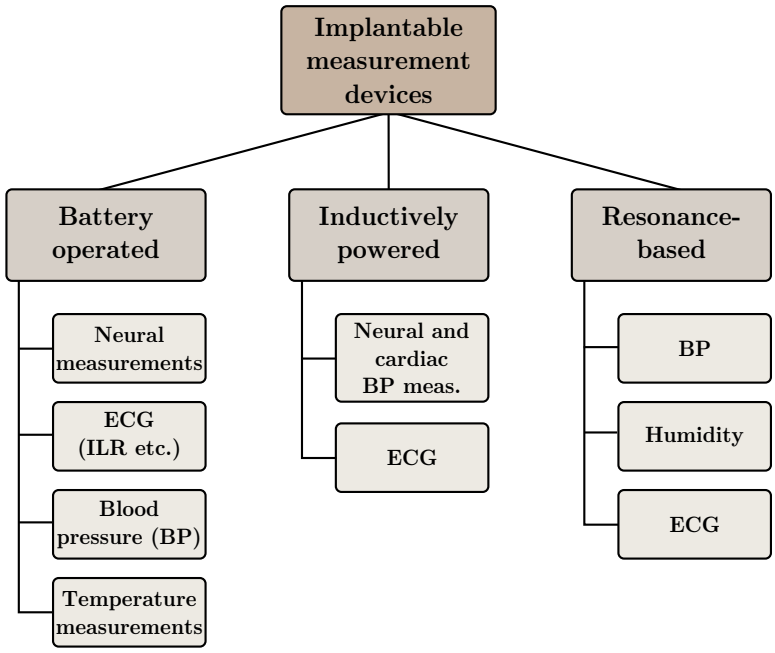

Fig. 4.1. *A block diagram of the three implantable device groups discussed in the text together with the applications related to these groups.*

4.1.1 Battery powered devices

Neural measurements are difficult to be performed with the surface measurement devices partly due to the applicability of the measurement sensors on the skull surface and partly because of the devices attached to the proximity of the head of the subject disturbing the measurements. In his PhD dissertation Ming developed an implantable wireless neural recording system with a system-on-a-chip measurement unit and a receiver unit connected to a computer [75]. The developed measurement device was designed to measure electrical neural signals, e.g. extracellular neural action potentials and EEG and it was also tested *in vivo* with rats and found to be functional. The device used 900 MHz link to communicate with the measurement computer for data transmission.

Detecting heart malfunctions is not an easy task since the malfunctions are not predictable. Also taking patients in to a hospital during the survey period, is not a cost effective option.

An implantable loop recorder (ILR) has been developed to provide possibility to continuously measure the function of the heart and record the events by pressing a button [72]. According to a research by Farwell *et al.* , the usage of ILR will to some extent increase the overall quality of life of the patients with recurrent heart problems [24]. Krahn *et al.* have also proved the ILR to be a very efficient tool in obtaining clinical cause for the recurrent heart problems. In their study, 16 patients with the episodes were researched to whose problems no clinical explanation could be found with the traditional monitoring techniques. With ILR implanted, 15 of the patients had the episode during the surveillance period and in every case a diagnose was obtained and successful therapy was begun. [55]

From an article by Potkay *et al.* [94], a comprehensive review of implantable blood pressure sensors can be found. For scientific purposes, widely used implantable devices to measure the blood pressure are the ones manufactured by Data Sciences International (DSI) (http://www.datasci.com). The variety of the products provided by DSI include devices able to measure EEG, ECG, temperature and blood pressure. The DSI devices are of the active type and have battery lifetime up to 12 months. The batteries in the DSI devices are primary batteries so that they cannot be recharged. The sensors, pressure sensors and electrodes, of the measurement devices, can be placed both on the surface of the heart and inside of it. A research conducted by Malpas, however, suggests that devices where the battery can be inductively loaded during the research provide more flexibility and longer duration to the research [64]. Implantable devices able to measure the same variables as the previously mentioned DSI devices but which can be inductively recharged are provided by Telemetry Research (http:// www.telemetryresearch.com/).

Valdarstri *et al.* have reported of an implantable measurement device that is able to measure the temperature and blood pressure [122]. The device communicates with an external receiver through a ZigBee radio operating at 2.4 GHz, incorporating a horizontal loop antenna which is found to be the most effective option for a subcutaneous RF-antenna [51]. What is surprising in the results of the research, is that the device was implanted 3–4 cm deep but still error less signal was obtained with relatively low transmission power, only 31.6 μW. It has been previously reported that operating at mid-UHF or low-GHz range is needed to be able to obtain several centimetres penetration of RF-signals in tissues [121].

4.1.2 Remotely powered devices

Passively functioning implantable devices are typically powered up over an inductive link between an external reader device on the surface of the skin and a subcutaneous measurement device. The ultrasonic powering of the implantable devices has also been researched but the sensitivity of the transmitted ultrasonic power to the matching of the acoustic impedance of the transmitter and the skin limits the applicability of this technique [3].

Eggers *et al.* have presented an implantable device to measure intracranial pressure which is powered through an inductive coupling [22]. The device is coated with a silicone elastomer and it incorporates an integrated receiver coil with dimensions of 5 x 5 mm that is made of electroplated Au layer on a silicon substrate. The telemetry unit was originally developed by Dudenbostel *et al.* [20]. Najafi *et al.* have also presented a similar kind of an implantable MEMS pressure sensor to measure blood pressure from a vein. The device was tested *in vivo* in canines [81]. The operating distance being less than 3 cm was found to be too short for the convenient usage of the device.

Enokawa *et al.* have presented an implantable measurement device to measure the ECG and the sympathetic nerve signals of small sized animals [23]. Their measurement device consists of a PC where the measurement data is stored and analysed, a backpack for controlling the implant and communicating with the computer and the implantable measurement device. The implantable device is powered with a 200 kHz magnetic signal with the aid of two coils, one in the backpack and one in the measurement device. The measurement data is transmitted through another inductive link from the implant to the receiver in the backpack. The research team have verified the function of the device on rats by *in vivo* tests and reported them in [23].

The inductive link determines the efficiency and operating range of the implantable measurement system. In order to optimise the efficiency of the inductive link, the coils forming the link should be optimal. There are some fundamental rules for optimal coil geometry, as presented e.g. in [36], but the complete optimisation of the coils is difficult in real life situations for example due to movement and therefore changing the distance and possibly also the geometry of the coils. Donaldson *et al.* have examined the complexity of coil optimisation and reported it successfully in [19]. Ko *et al.* have presented a design procedure for optimally coupled coils when certain border conditions related to the geometry of the coils are known [53].

The mutual movement of the resonating coils is a problem in applications where the external device is wished to be portable. The movement between the coils causes variation in the coupling coefficient of the coil pair and thus also variation in the induced voltage at the implantable device. Furthermore, variation causes depth variation in the reflected signal which deteriorates the received signal if amplitude coding is being used. Van Schuylenbergh *et al.* have proposed means to compensate for the mutual movement of the coils to regain optimal signal over wider range of measurement distances [125]. According to their idea, a second coil is introduced in the reader device which senses the load modulated signal reflected from the implantable device. The other coil is used for power transmission. A constant tuning of the power supplying frequency is possible because of the two coils used for power and data transmission and the link can be held functional from longer distances than without the tuning circuitry. Van Schuylenbergh *et al.* used 1 MHz frequency in their experiments and

obtained operation distances up to 70 mm for reliable data transmission. Zierhofer *et al.* have reported on enhanced coupling coefficients between two inductive coils when the coils are not concentrated on the circumferences of the coils but are distributed over the radius of the coils [135, 136].

An important and interesting method to construct coils for applications where the applied frequencies are in the order of tens of megahertz, is constructing the coil on the substrate of the device. The substrate may be a printed circuit board (PCB) or a silicon substrate. Yue *et al.* have published a paper on the modelling of spiral inductors made on silicon substrate [133]. Sunderarajan has also successfully presented methods to mathematically calculate and simulate on-chip inductors in his PhD thesis [112]. He also designed optimal spiral coil structures functioning at 2 and 3 GHz. With a careful design of the resonating coils, very high power can be transferred wireless. Kurs *et al.* have reported of powering up an 60 W incandescent lamp from a 2 m distance utilising four coils [57].

4.1.3 Resonance-based devices

The measurement principle in the resonance-based devices is relying on an inductive coupling between an external detector and a sensor. The sensor can be either on the skin surface or it may be implanted. The two devices are inductively coupled with each other through the coils on the devices. The sensor does not contain any active electronic components, but it consists only of an LC-tank with a resonance frequency f_0. The LC-tank is constructed of capacitive and inductive components with at least one whose value is able to vary as a function of the measured quantity. The inductive connection between the reader device and the sensor together with the reflected impedance from the sensor is shown in Fig 4.2.

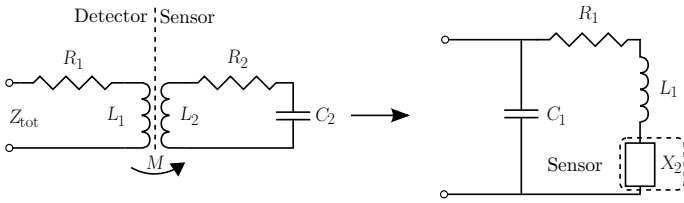

Fig. 4.2. *Schematic figure of the measurement principle with the resonance sensor. One of the secondary circuit (sensor) components, C_2, L_2 or R_2, may change as a function of the measurement quantity.*

The changes in the measured quantity may change the value of one of the passive components, C_2, L_2 or R_2, at the sensor. While one of the values change, the others remain fixed. The changes in the component values at the sensor will alter the reflected impedance of the sensor. The right hand side of Fig 4.2 illustrates how the impedance of the sensor will be reflected and seen at the detector. The equations to calculate value for X_2 can be found e.g. in [1, 36,

39] and from P5. When the reflected impedance of the sensor changes, it also changes the resonance frequency of the detector circuit. By measuring the resonance frequency of the detector, the value of the reflected impedance, and hence the value of the varied component at the sensor can be calculated. The signal transmission method is called load shift keying (LSK) and it is handled in more detail in an article by Tang *et al.* [117].

The resonance frequency of such a system is typically set to several megahertz due to smaller physical dimensions of the coils at these frequencies [121]. Harpster *et al.* present in their article a good illustration about the influence of different geometrical and electrical factors to the depth of the resonance [39].

A passive humidity sensor based on the resonance effect between a reader device and a separate LC-tank has been presented by Harpster *et al.* in [39]. A capacitive humidity sensor is being used in the application as the frequency shifting component in the sensor. The resonance frequency of the system was set to lie between 17–18 MHz and the signal was possible to read only from a very close proximity of the sensor. The measurement distance with a ferrite core coil was only 1 cm. The humidity sensor was tested *in vivo* in guinea pigs to monitor the hermeticity of the implanted package [38].

A resonance-based pressure sensor has been developed and presented by Akar *et al.* in [1]. The pressure is measured by using a capacitive pressure sensor made of silicon. The operating frequency of the device is at 70–75 MHz. Takahata *et al.* have designed an implantable resonant pressure sensor which is implanted with an angioplasty stent [115]. The stent itself is made of 50 μm thick stainless steel foil by laser cutting and the structure is designed so that controlled fractions will occur at certain places thus forming a coil as the angioplasty balloon is inflated. The operating frequency of the device is around 201 MHz when it is operated in a liquid ambient.

All the resonance-based devices presented so far have been based on measurement of mechanical quantity, the blood pressure. However, also biopotentials can be measured utilising the resonance sensing technique. Towe has presented in his paper [121] a measurement device based on the resonance effect where the secondary circuit values are changed by a varactor, i.e. a variable capacitance diode. The operating frequency of the sensor was 300 MHz. The voltage difference between the electrodes connected to the test person is used to variate the capacitance of the varactor and the biopotential can be measured. In his paper, Towe demonstrated the functionality of the measurement device by measuring the ECG signal. The same kind of measurement device has been constructed and presented in P5 yet various detection methods are presented in more detail in the latter paper.

Karilainen *et al.* have presented an alternative approach to measure the biopotentials using a varactor. The measurement system proposed in [48] is based on the same kind of a loading circuit as discussed earlier, whose impedance can be changed by a potential coupled between electrodes that are connected over a varactor. The coupling between the sensor and the reader

device of the proposed measurement system is, however, different from the ones presented in P5 and [121]. The coupling of the sensor to the reader, or interrogation device, is realised by interdigital transducers (IDT). The IDT of the sensor is coupled to a surface acoustic wave (SAW) delay line which also contains two other IDT. The first of these two IDT is used as reference to compensate for the transmission line effects and it can also be used to distinguish between several separate sensors. One interrogation unit is capable of reading six sensors at a time. The second IDT at the end of the delay line will reflect back the incoming signal modified by the varying impedance of the load circuit. The biopotential can be read at the interrogation unit from the reflected signal. The sensor structure and optimisation are also presented in [49] and the design and properties of the interrogation unit in [25].

4.2 Material considerations for implantable applications

The implantable devices meet a very challenging environment. The materials to be used in the devices have to be such that the tissue response evoked by them remains minimal. When a material shows a minimal tissue response, it is called a *biocompatible* material. Geddes *et al.* have listed four important factors to be taken into account with the implantable (electrode) materials: 1) tissue response, 2) allergic response, 3) electrode-tissue impedance, and 4) radiographic visibility. [32]

The measurement and stimulation devices meant either for biopotential measurement or stimulation of muscles based on biopotential data, both traditionally need a galvanic contact to be built between the device and the tissue. The device itself must be hermetically coated with a biocompatible material and but the electrodes shall remain uncoated. The electrode material has to be chosen so that it is biocompatible with the tissue.

Some of the electrode materials that are suitable for surface measurements are not suitable for implantable applications. Good examples of such materials are e.g. Ag/AgCl which is widely used in surface electrodes and Ag. The AgCl-layer is found to dissolve into the tissues causing severe inflammation in the tissue surrounding it [77]. Pure silver has been widely used as antibacterial material in many applications [50]. However, pure silver has also been proved to be extremely toxic to the tissues when implanted [99].

Collias *et al.* conducted an extensive research on implantable electrode materials [15]. In the research, they implanted several electrodes made of stainless steel into the brains of cats. Their study consisted of many phases where they studied the tissue reactions caused by the electrodes. After four months of implantation, all the electrodes were tightly surrounded by a thick, dense fibrotic capsule. Despite the fibrotic capsule formation, stainless steel was regarded as biocompatible material suitable for long term implantation. Stainless steel has also been widely used in other, often mechanical applications that are implanted, e.g. in screws closing the sternum after an open-heart operation [47].

In addition to stainless steel, also gold (Au) and platinum (Pt) have been found to be biocompatible [10, 99, 110]. Pt and Au show good biocompatibility when used in measurement purposes. When the stimulation of nerves or muscles is desired, Au will easily be corroded due to high current density at the interface. Pt show better stimulation capability due to its capability of not being corroded under high current density. [10]

Titanium (Ti) is a widely used material in the cans of the implantable devices, e.g. pacemakers. Ti has an excellent compatibility with the tissues. It also forms an oxide layer on the surface which makes the material even more susceptible to corrosion [10, 21, 111]. Zhang *et al.* have presented in their paper that the TiO_2 material has also properties that are favourable in blood contact. The TiO_2 coated low-temperature isotropic pyrolytic carbon showed much less trombus on itself than the uncoated material [134]. Ti electrodes are not widely used but as in all measurement applications, the current density on the electrode surface remains small, which corresponds to almost a static or non-electric application where the corrosion tolerance of Ti is known to be excellent.

4.3 Inductively powered ECG monitor: Device characterisation

An inductively powered, implantable measurement device for continuous, wireless, one channel ECG measurement was designed and constructed at TUT. Altogether, four different prototypes were constructed that were tested *in vivo* in cows. The number of test animals varied between the *in vivo* tests from four to eight. All the *in vivo* experiments were done under a valid animal experiment licence granted to the MTT Agrifood Research Finland by the Finnish animal experiments committee.

The first prototype of the device is presented in detail in P4. P8 also partly presents prototype number one, yet some enhancements were done to the first *in vivo* tested prototype, P4, e.g. the coil was changed from a commercial coil to a handmade coil to enhance the coupling. P9 presents the third prototype of the implantable ECG device. The third prototype was constructed on flexible PCB utilising folded-flex structure. The folded-flex structure enabled the miniaturisation of the developed device. Fig 4.3 shows a photograph of the four prototypes tested *in vivo* in cows.

During the development process of the devices, several metallic materials to be used as electrodes were under test to find out their electrochemical properties when in contact with a liquid electrolyte. The solution simulated the implantation conditions. These studies were discussed in more detail in Section 3.3.2. Also the biocompatibilty issues of the electrode materials were of interest and were studied during the process. These issues were discussed from the material science point of view in Section 4.2. The designed and realised prototypes of the implantable ECG measurement devices will be shortly revised in this section.

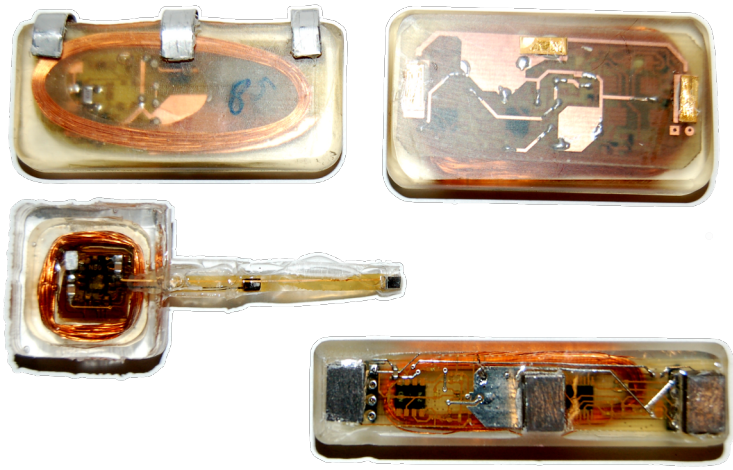

Fig. 4.3. *In vivo tested implantable ECG monitoring devices realised at TUT. First prototype at the high left corner, consecutive versions running row-wise.*

The implantable ECG measurement device was designed to be used in monitoring of cows' well-being. The manufacturing process of the implantable device faced two border conditions. The first constraint was that the design and the prototype construction process should not demand any special facilities or process steps. This both speeds up the prototyping and lowers the costs of the prototypes. Second border condition was that the device was to be inductively powered from an external reader device and the same link was to be used for the data transmission. The operating frequency of the link was set at 125 kHz. The relatively low operating frequency of the link, for comparison see e.g. [46, 57], was used because a commercial transponder integrated circuit (IC) by Atmel (U3280M) was used in the device which had a specified operating frequency at 125 kHz. The chosen transponder component was used due to its internal voltage regulation possibility. The internal regulation capability of the transponder decreased the number of components and current consumption of the prototype device. An alternative solution would have been to use either a fixed reference diode or an adjustable voltage regulator.

The low operating frequency of the device introduced challenges in the coil design and optimisation. Low operation frequency means great dimensions of the coil but the coil in the implant could, however, be made to meet the size demands set by the implantation conditions. The coils were designed to be flat as suggested by Zierhofer *et al.* in [135] to get optimal coupling between the reader and the implantable device. Operation distances in the air for the four versions varied between 38–70 mm (first and fourth prototype).

The electrode material used in the prototype versions number one and three was AISI 316L, a.k.a. surgeon steel, in prototype number two Au and in prototype number four Ti. The

electrodes were arranged so that the outermost electrodes were the two potential sensing i.e. measuring, electrodes and the electrode in the middle was used to set the zero potential of the measurement device. The distance between the middle points of the measuring electrodes varied between 43–60 mm, being the shortest in the first prototype and longest in the fourth prototype. The mutual electrode configuration was the same in every prototype.

4.3.1 In vitro *tests of the implantable ECG monitors and results*

Prior entering the *in vivo* tests with the implantable ECG-measurement devices, some *in vitro* tests were being made. The tests were done with the first prototype but since the schematic of the electronics design of the third and fourth prototype was the same as with the first prototype, there was no need to repeat the tests with the other prototypes.

The first *in vitro* tests were carried out in a plastic container filled with saline. The tests are reported in detail in P4 where also the result graphs are shown. The conduction and results of the tests are reviewed here. The ECG monitoring device was fixed at the edge of the container and a sinusoidal signal was fed into the solution using two wire electrodes made of Ag and the response measured by the implantable device was measured from the outside of the container. This test served two purposes:

1. Prior to the implantation of the device into cows, it was needed to show that the measurement of potential fields is possible when the measurement device is immersed in a highly conducting media and completely surrounded by it.

2. By using a sinusoidal input with frequency 20 Hz, it is possible to see how much distortion the finite sampling rate ($f_s = 237$ Hz) of the measurement device will cause to the measurement signal. The input frequency of the test signal was chosen to lie on the half-way of the information band of the human ECG signal [114]. Based on the knowledge gained from previous experiments with surface measurement devices on cows, the information in the cow-ECG was known to approximately lie on the same interval.

The second *in vitro* test was performed with the measurement device placed on the skin of a test person. The test was almost an *in vivo* test with realistic human-ECG signal yet the device was not implanted. The second *in vitro* test was done to find out the performance of the device with ECG-signal and to compare the signal quality given by the electrodes used to their commercial counterparts. The measurement device was held on the test person's skin surface at the midclavicular line extending over the second and fourth rib bones. The place is identical with the implantation site of the Medtronic Reveal Plus ILR. Measuring the ECG with the proposed measurement device at the same place gave a good indication of the performance of the device. The measurement device used electrodes made of surgeon

steel, AISI 316L, and they were tested against commercial Blue Sensor wet gel electrodes by Ambu A/S made of Ag/AgCl.

The sinusoidal signal measurement from the saline showed that the device is able to measure the 20 Hz potential signal from the liquid environment without disturbances and send it further to the reader located 11 mm away from the implantable device. This ensures data and power transmission to and from the implant in *in vivo* circumstances.

Furthermore, the measurements done with the implantable device on the skin surface showed that the device is sensitive enough to record the ECG signal from the skin surface, Fig 4.4. According to a research by Väisänen *et al.*, the signal amplitude is assumed to be a few percent greater when being measured with an implantable measurement device than from the skin surface although the difference with a few millimetres implantation depth is not dramatic [129].

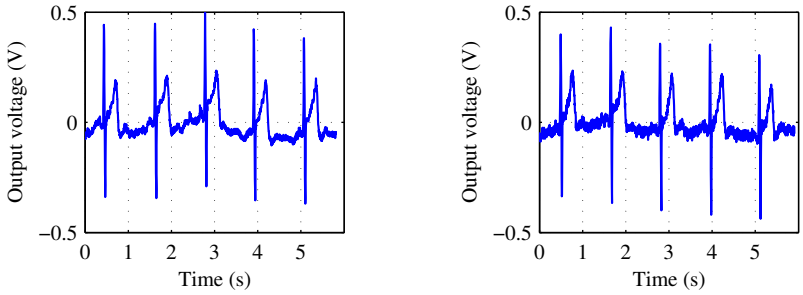

(a) Blue Sensor electrodes.

(b) AISI 316L Surgeon Steel electrodes.

Fig. 4.4. *Signal output of the implantable ECG measurement device when placed on the skin surface at the midclavicular line extending over the second and fourth rib bones.*

The AISI 316L electrodes showed slightly higher SNR in the test measurements compared with the commercial ones. Unlike reported in P4, a more accurate analysis of the SNR showed that for AISI 316L steel electrodes the SNR was 74.6 dB and for the commercial Ag/AgCl electrodes it was 73.2 dB. The difference between results presented in P4 and here is due to larger amount of data that was used in reproducing the results. Also the calculation principle of the SNR was slightly different. The higher SNR obtained with the steel electrodes is due to the calculation method of the SNR whereby the dynamic range of the signal is referred to the peak-to-peak amplitude of the noise signal and because of the nature of the steel and Ag/AgCl electrodes. As discussed in Section 2.3, the Ag/AgCl electrodes are close to non-polarised electrodes and the steel electrodes are more like polarised electrodes in their nature. Thus the steel electrodes exhibit stronger capacitive behaviour in their electrical equivalent as suggested in Fig 2.3. Greater capacitive component in the interface of the steel electrode

will function as a high-pass filter which lets the QRS-complex to be recorded with higher amplitude than with the non-polarised, almost completely resistive Ag/AgCl-electrodes.

4.3.2 In vivo *tests of the implantable ECG monitor and results*

In vivo experiments were conducted with all of the four presented prototypes of the implantable ECG measurement device shown in Fig 4.3. In every *in vivo* measurement, the implantable devices were implanted into the left side of the cow into a subdermal pocket which was sutured with two sutures. The length of the implantation periods varied from 24 hours to 15 days. More specific measurement setup and results of the first *in vivo* experiments are reported in P4. The effect of the orientation of the measurement device was studied under the first *in vivo* experiments. There were in total four different alignment possibilities for the implantable device:

1. Electrode array positioned horizontally, parallel to the cow spine, electrodes towards the body of the cow, antenna coil towards the skin of the cow.
2. Electrode array positioned horizontally, parallel to the cow spine, electrodes towards the skin of the cow, antenna coil towards the body of the cow.
3. Electrode array positioned vertically, orthogonal to the cow spine, electrodes towards the body of the cow, antenna coil towards the skin of the cow.
4. Electrode array positioned vertically, orthogonal to the cow spine, electrodes towards the skin of the cow, antenna coil towards the body of the cow.

Based on the measurement results presented in P4, orientation number 1 was considered as the best due to the highest SNR although the R-spike amplitude was highest with orientation number 3. The difference between the SNR of orientations 3 and 4 was negligible but between orientations 1 and 3 substantial (7 dB). Alignment possibility number 2 was not tested since the results from alignments 3 and 4 suggested the SNR to remain the same but the R-spike amplitude would be halved compared to the amplitude of measurement with alignment number 1. Hence, in the consecutive *in vivo* tests, alignment number 1 was used for all the implanted measurement devices.

The second *in vivo* experiments were unfortunately unsuccessful. The power and data transmission to and from the implantable device was functioning perfectly but the device did not measure the ECG signal. The reason for this was later found out to be the conductive adhesive used to fixate the Au-electrodes onto the PCB of the device. The adhesive was slightly out of date but was regarded to be in sufficiently good condition to be used in the prototype to create the electrical connection between the electrodes and the PCB. This deduction was

based on the *a priori* information obtained from earlier studies made with the adhesive. An example of the measurement signal obtained with the third prototype device is reported in P9.

The measurement results made with the fourth prototype are shortly presented in the thesis. The fourth *in vivo* measurements made with the cows were the most successful in terms of the measurement data quality (SNR, lack of disturbances) due to the best electromechanical design of the implant and longest implantation time. The design of the fourth prototype can be seen in Fig 4.3 in the lower right corner. The electrodes used in the prototype were made of Ti and had the largest geometrical area, 6 x 9 mm. The electrodes were also slightly higher than the coating of the implant to secure a good electrical connection with the tissue.

In the previous *in vivo* tests, it was noticed that the operated area is filled with tissue fluids and the skin is sensitive to touching. The tissue fluids can easily short circuit the electrodes with each other and the biosignal is hard to measure. Furthermore, when the skin is sensitive for touching, touching the skin from the surface causes the cow to rub her skin and the implant moves inside the subdermal pocket. This causes motion artefact in the measurement signal and the electrochemical stabilisation process begins again from zero as learnt in Section 2.6. The cow skin is easily touched when performing the measurements since the coil of the reader device has to be brought close to the skin to obtain adequate signal levels. Therefore in the fourth tests, a five days time gap was held between the implantation and starting of the measurements. Fig 4.5 shows an example of the raw measurement signal and two examples of the signal where the time scale is reduced to an interval of two seconds to better distinguish the characteristics of cow ECG.

From the measurement results it can be seen that already the raw data with the DC-offset reduced is fairly good and the inductive link between the reader and the implant has been able to be kept successfully on for almost two minutes in a row. The result indicates that the electrodes have a good contact with the tissue and the operated region of the cow has been healed properly. Also the cow does not find the measurement situation uncomfortable thus the inductive link has been easy to be held on. Typically the link is broken down due to the cow movements.

By bandpass filtering the signal with a 2^{nd} order Butterworth filter with pass-band at 2–20 Hz and narrowing the time window, the ECG of the cow can be easily seen in the figure with the clearly distinguishable R-spikes. A narrower pass-band than the information band of the ECG signal [114] was chosen since the signal characteristics can be seen clearest from the resulting signal. The R-spikes are rounded at the tops a little with this filtering method but the R-spike location can still be easily determined.

The *in vivo* measurements in general, however, indicated that the inductive link is too sensitive to the movements of the subject (cow) and the link is easily turned to off state during which the measurement is not possible. This causes problems in retaining the time scale

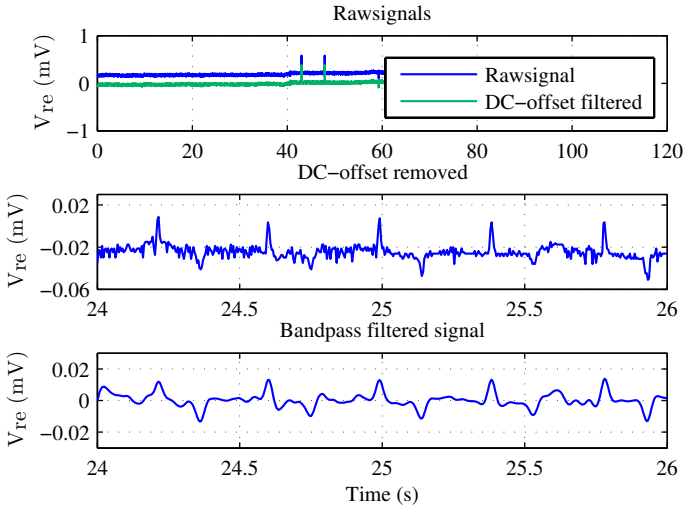

Fig. 4.5. *Measurement result of cow ECG with implantable ECG measurement device prototype number four. At the top the raw signal is shown with the raw signal where the DC-offset has been removed, the raw signal with reduced time interval in the middle and signal filtered with 2nd order Butterworth filter with pass-band at 2–20 Hz at the bottom. 'V_{re}' is an abbreviation from 'Voltage reduced to electrodes'.*

constant throughout the measurement which is crucial with respect to the analysis of the ECG signal, e.g. heart rate variability (HRV) analysis. Therefore the measurement system and setup as such are not reliable or usable enough to perform large scale *in vivo* tests with animals. Modifications regarding the design of the inductive coils to enhance their mutual coupling coefficient and misalignment tolerance should be made if not completely go over to battery powered devices with radio links. The electrode setup (size, material and positioning) of the fourth prototype was found to be the very functional and together with the longer operation–measurement interval, the measurements were easier to perform and the results were also more reliable than in the previous *in vivo* tests.

4.4 Resonance-based passive biopotential (ECG) measurement device: characterisation

In addition to using an inductive link to power up measurement devices from a distance, Section 4.1.2, the link can also be used in accordance with resonance-based measurement devices, Section 4.1.3. The measurement schemes presented here can be used both in implantable applications and in surface measurements.

A measurement device based on the change of the resonance frequency of an LC-tank that is

able to measure biopotentials either from the skin surface or as implanted, has been realised at TUT, P5. Towe has also published a paper about a similar measurement device [121]. P5 provides, however, more insight into the measurement techniques related to the detection of the varying resonance frequency and reflected impedance of the LC-tank than discussed in [121].

The realised measurement device is based on the operation principle shown in Fig 4.2. There are at least two possibilities to construct the sensor circuitry. The two alternative ways of constructing the measurement circuitry mostly differ from each other in the number of varactors used in the sensors. Fig 4.6 illustrates the two possible schematics of the resonance sensor where BBY40 varactor by Philips Semiconductors. The BBY40 was chosen because according to the data sheet it was specified to be able to operate around zero volts which is the case for ECG measurements and a PSpice simulation model was also provided which enabled theoretical simulations to be run for the measurement setup. The version shown in

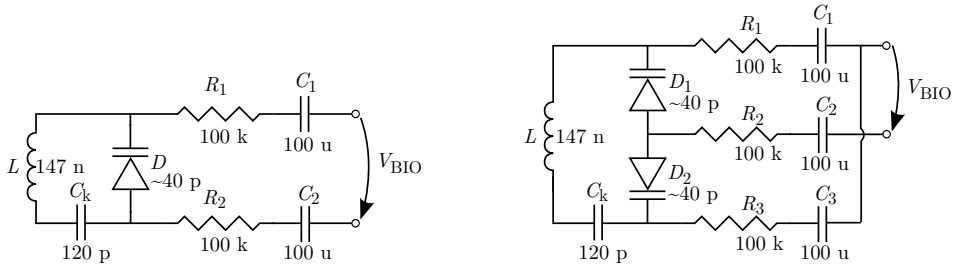

(a) Version with one BBY40 variable capacitance diode.

(b) Version with two BBY40 variable capacitance diodes.

Fig. 4.6. *Schematic figure of the sensing unit with BBY40 variable capacitance diodes.*

Fig 4.6(b) has the advantage that the relative total capacitance change of the sensor circuit is larger than for the sensor shown in Fig 4.6(a) in the case where the capacitance of the varactor is changed by the biopotential. The difference will not be great, yet substantial, so that the usage of the circuit shown in Fig 4.6(b) is encouraged.

Reading of the signal (reflected impedance) at the reader device has been realised using two different kind of measurement devices. First of these devices was a slope detector that was simpler to implement than the second reader device where the sensing principle relied on phase-locked detection.

The detection principle in the slope detector was to measure the impedance magnitude of the reader device at some definite frequency. Changes in the capacitance of the varactor will change the impedance of the sensor and the total impedance of the reader device will change due to the changes in the reflected impedance. The magnitude of the total impedance will reflect the potential that has been measured at the sensor. The schematics of the realised slope detector is illustrated in Fig 4.7(a).

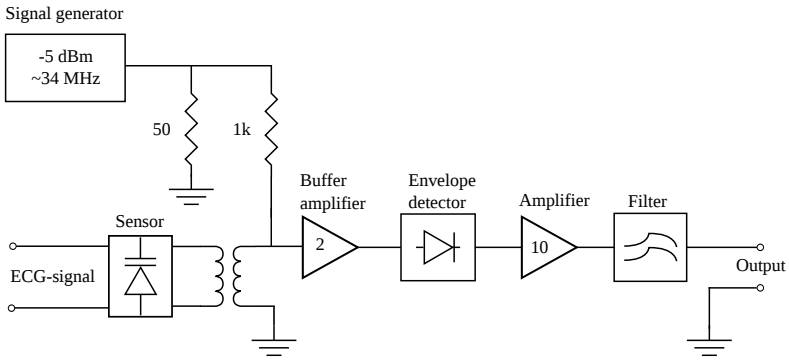

(a) Schematic figure of the slope detector.

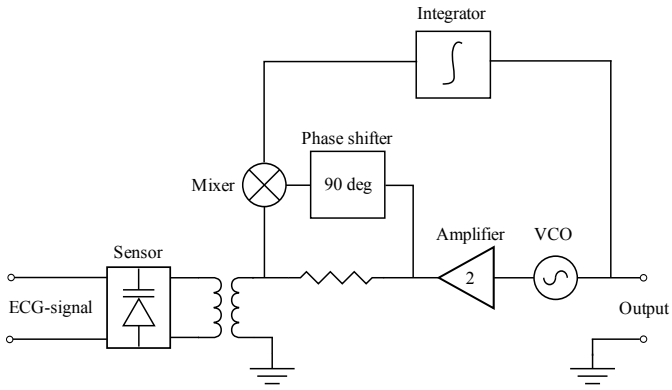

(b) Schematic figure of the phase detector.

Fig. 4.7. *Schematic figures of the resonance sensor measurement devices. Figures originally published in P5.*

Another possibility for the signal readout is to use a phase-locked detector which according to [49] provides better SNR of the measurement result. A schematic of the measurement device is presented in Fig 4.7(b).

The measurement principle in the phase-locked detector is that a sinusoidal signal is fed into the coil of the detector. The reader is locked at zero degrees of the sensor reflected impedance which means that the reader is operating at sensor's resonance frequency.

The VCO shown in the diagram feeds an oscillating signal to the phase shifter where it is shifted by 90° prior entering the mixer. The mixer's other input is coupled to the reflected impedance from the sensor and it is resonating at a frequency determined by the LC-resonator of the sensor. The two signals are mixed at the mixer and the outcome is a sinusoidal signal with a DC-bias. If both the input signals are in the same phase, the output DC will be at 0 V_{dc} but if there is a difference in the phase, the output will have a non-zero DC level which will be integrated into a DC potential. The phase difference is caused by the tank when the induced

frequency is different from the resonance frequency of the tank. DC-voltage will be used to control the VCO which together with the feedback loop will try to retain the input of the integrator at 0 V which means that the VCO is kept at the resonance frequency of the sensor. The resonance frequency of the secondary circuit, the sensor part, can be deduced from the control voltage of the VCO hence the output of the sensor system is the control voltage of the VCO.

4.4.1 Measurement results

The resonance measurement device was tested by attaching commercial surface electrodes (Blue Sensor by Ambu A/S) on the skin of a test person. Both detector devices presented in Section 4.4 were used in the measurements and the measurement results were in the first stage referred to results given by a battery-powered biopotential amplifier. The two measurement electrodes were placed on the upper thorax and the measurement lead was directed so that it was parallel to the electrical axis of the heart. Placing the electrodes this way maximises the R-spike strength (amplitude). One of the electrodes was placed just beneath the clavicula on the right side of the thorax and the other was placed on the left side of the thorax in the 7^{th} rib bone gap. The electrode configuration was very close to being the aVR-lead led from the Einthoven's triangle [63]. The electrodes were connected to the sensor unit with unshielded cables. The coil used in the detector device had an average diameter of 25.5 mm and the sensor coil had an average diameter of 13.5 mm.

The measurement results compared against the results given by the reference device clearly indicated that the device and both the detectors are working properly and are able to measure the ECG signal reliably. The performance of the detectors was then further tested as a function of coaxial distance between the detector and sensor coils and also as a function of the coaxial misalignment between the coils. Fig 4.8 shows the measurement results obtained with the slope detector and Fig 4.9 presents the results of the measurements obtained with the phase detector when the coaxial distance between the coils was altered. The slope detector was not able to measure the ECG above measurement distances of 50 mm. The phase detector was, however, able to measure the ECG up to 55 mm. The measurements clearly indicate that the quality of the signal measured with the slope detector is not as good as with the phase detector when the coaxial distance between the coils varies. Table 4.1 further indicates the problems the slope detector is suffering: The SNR of the signal measured with the slope detector varies dramatically as a function of the coaxial distance being highest at 23 mm and 40 mm, which lie on the interval on which the coils electrical matching is optimal. The SNR does gradually alter in both ends of the measurement range. The phase detector signal does not suffer from remarkable degradation as a function of the coaxial distance, instead the SNR remains almost constant throughout the measurement range.

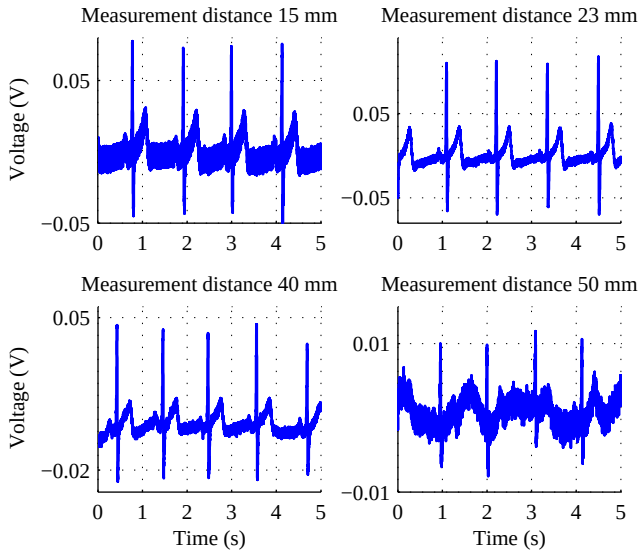

Fig. 4.8. *Measurement result of ECG obtained with the slope detector when the coaxial distance between the detector and the sensor coils is altered. Figure originally published in P5.*

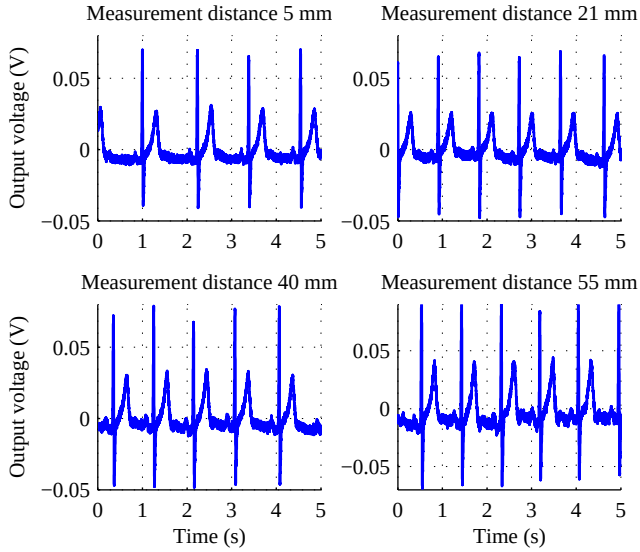

Fig. 4.9. *Measurement result of ECG obtained with the phase detector when the coaxial distance between the detector and the sensor coils is altered. Figure originally published in P5.*

The coaxial misalignment tolerance of the detection devices was also under research. The results showed the same tendency than those measured with the different coaxial separations:

Table 4.1. *SNR of the measurements done with the slope and phase detectors. The results include both coaxial and lateral separation of the coils. Data originally published in P5.*

Slope detector		Phase detector	
Coaxial separation			
Distance (mm)	SNR (dB)	Distance (mm)	SNR (dB)
15	36	5	59
23	65	21	59
40	56	40	62
50	33	55	56
Lateral misalignment			
Misalignment (mm)	SNR (dB)	Misalignment (mm)	SNR (dB)
10	61	10	58
35	38	25	57

The slope detector suffers from a gradual degradation of the measurement signal quality, hence also poorer SNR, as the misalignment is increased.

5. DISCUSSION AND CONCLUSIONS

Electrode characteristic properties have been studied and reported. Theoretical background has been provided to the interface properties of the electrode–electrolyte interface. The interface properties have also been researched experimentally with measurements. The measurement setups and results have been presented in detail in P1, P2, P6 and P7.

The measurement of the electrode–electrolyte interface properties is essential in acquiring knowledge about the electrochemical behaviour of the electrode. The measurement results also serve as a guideline in determining suitable electrodes for the current purpose. The properties that influence the suitability of an electrode material are e.g. electrochemical noise arising from the interface and the electrical equivalent component values of the interface. These issues have been researched in P1 and P2 for metallic electrodes that have been immersed in different electrolytes. Also, P7 reports measurement results obtained from similar kind of measurement setups. P6 discusses the RMS-noise arising from the interface together with the impedance measurements of textile based electrodes.

Results of the RMS-measurements with metallic electrodes immersed in various electrolytes, P2, showed that the electrolyte conductivity and constituents have their effect on the sensed electrochemical noise arising from the interface. The Ag/AgCl electrodes that are traditionally regarded as stable and low noise electrodes showed surprisingly higher electrochemical noise in almost all electrolytes than AISI 316L electrodes with equal area.

The textile electrodes are an interesting type of electrodes thanks to their good integrability into garments. Four textile-based electrodes made of different materials were studied on top of an Agar-block whose conductivity was fixed to meet that of a wet human skin. The conductive material of three of the electrodes was Ag and in the fourth the conductive material was Cu and Ag. The impedance of the Agar-block was in the order of 500 Ω at 100 Hz which is in the order of values that Grimnes has reported in [35] for the impedance of human tissues. The impedance of the skin should be much higher if it was not prepared, e.g. scratched, as reported by Rosell *et al.* in [101]. The RMS-noise measurements were performed as a function of time to obtain a reliable measure of the stabilisation time of the electrode–electrolyte interface. It seemed that 10 minutes after the application of the electrode on the subject, the interface is stabilised at its long-term low-noise level. The preliminary conditioning of the electrode materials was also under research. Three different scenarios were tested: uncon-

ditioned electrodes, hydrogel membrane enhanced electrodes and electrodes moistened with PBS. The measurements showed that the PBS moistened electrodes provided the most stable measurements and shortest stabilisation times despite the material.

The impedance measurements were performed in P1 and P6 with the square wave method presented in detail in Section 2.8. The method enables the determination of the component values of the electrical equivalent circuit of the interface, e.g. in Fig 2.4(a), without the need for expensive laboratory equipment such as an EIS device. First the measurements were performed on the metallic electrodes immersed in liquid electrolytes. The results showed that the measurement method is applicable to the measurement of the electrode–electrolyte interface component values and the results it gives are in line with those obtained by other scientists. The same measurement method was applied to the textile electrodes and found to give correct results also there. Comparison between the component values between the metallic and textile electrodes revealed that the textile electrodes were more non-polarised electrodes than the metallic ones partly due to their material (Ag or Cu) and partly because their effective area is much higher than for the metallic electrodes. Higher effective area lowers the interface resistance value calculated for one geometric-cm^2.

The knowledge about the electrodes can be applied to the measurement devices presented in P3, P4, P5, P8 and P9. All the publications mentioned discuss the biopotential measurement devices that need electrodes to be able to measure the signals. Knowledge is especially needed in the implantable applications where the electrode material has to be biocompatible and thus, harmless to the tissue. In addition to this it should not attenuate or filter the biosignal drastically.

An implantable, inductively powered ECG measurement device has been introduced for the first time in P8 and both *in vitro* and *in vivo* measurement results are reported in P3, P4 and P9 together with technical data about the various versions of the devices. The devices have been proved to be implantable and causing no inflammations to the cows where the devices have been implanted. With such an implantable device it is possible to collect long term data from the animals where traditionally the surface electrodes have been a problem. The reliability of the inductive link in the devices should be, however, enhanced to be able to record longer periods of ECG data from the animals.

In publication P5 an alternative way to construct a biopotential measurement device has been presented. The device is based on an LC-tank whose resonance frequency can be adjusted by modulating its capacitance with a varactor with electrodes connected over varactor ends. When the electrodes sense a biopotential, the capacitance value of the varactor is changed and, thus, also the resonance frequency of the sensor alters. The change can be detected with a detection device and transformed into equivalent voltage. The device has been constructed and tested with surface electrodes attached to a human skin. The measurement results were promising but the device still suffers from artefacts caused by the alternating distance between

the sensor and the detector. Compensation circuitry should be designed to compensate for the movements. The measurement device is extremely simple and inexpensive to manufacture and, thus, it would be an optimal choice to be used as a disposable sensor. The advantage the sensor has lies in its wireless and simple nature. The subject of measurement can be totally free of measurement wires, only the electrodes connected to the sensor and the sensor itself have to be attached to the subject. Also, if the measurement device is to be implanted, the extremely simple structure of the sensor enables it to be placed in places where the size of the sensor is an issue.

Implantable devices and resonance-based devices will certainly be available for the masses in the future. There are, however, some issues that have to be solved before the technology is ready to be commercialised. In the implantable devices, more attention has to be paid on the design and functionality of the inductive link. The link has to be more reliable for portable applications than it nowadays is. The reliability of the link also means longer operation distance. One option to overcome the challenges in the design of the link is to go over to use battery operated devices. The resonance-based device has to be enhanced in its ability to reject artefact arising from the varying distance between the sensor and the detector device. The distance variation could be compensated e.g. with a fixed LC-tank whose value would reveal the changes in the link properties.

BIBLIOGRAPHY

[1] O. Akar, T. Akin, and K. Najafi. A wireless batch sealed absolute capacitive pressure sensor. *Sensors and Actuators A*, 95:29–38, 2001.

[2] S. Aronson and L. A. Geddes. Electrode potential stability. *IEEE Transactions on biomedical engineering*, BME–32(11):987–989, November 1985.

[3] S. Arra, J. Leskinen, J. Heikkilä, and J. Vanhala. Ultrasonic power and data link for wireless implantable applications. *2nd International Symposium on Wireless Pervasive Computing, 2007. ISWPC '07*, pages 567–571, February 2007.

[4] O. Aumala, H. Ihalainen, H. Jokinen, and J. Kortelainen. *Mittaussignaalien käsittely*. Pressus Oy, 1998. 323 p.

[5] A. K. Barros, A. Mansour, and N. Ohnishi. Removing artifacts from electrocardiographic signals using independent component analysis. *Neurocomputing*, 22:173–186, 1998.

[6] L. Beckmann, S. Kim, H. Dückers, R. Lückhardt, N. Zimmermann, T. Gries, and S. Leonhardt. Characterization of textile electrodes for bioimpedance spectroscopy. *Smart Textiles–Technology and Design –Ambience08*, pages 79–83, 2008.

[7] S. C. Bera, S. Chattopadhyay, and B. Chakraborty. An experimental analysis of the non-linear behaviour of a bio-electrode polarisation impedance with excitation frequency. *Measurement*, 35:363–370, 2004.

[8] G. D. Bergland. A guided tour of the fast fourier transform. *IEEE Spectrum*, 6(7): 41–52, July 1969.

[9] J. Bronzino. *Biomedical Engineering and Instrumentation: Basic concepts and applications*. PWS Publishers, 1986. 481 p.

[10] P. K. Campbell and K. E. Jones. *Materials for Implantable Electrodes and Electronic Devices*, volume 14 of *Materials Science and Technology, A Comperensive Treatment: Medical and Dental Materials*, chapter 10, pages 345–372. Weinheim:VCH, 1992.

[11] O. Casas and R. Pallas-Arény. Electrostatic interference in contactless biopotential measurements. *IEEE Engineering in Medicine and Biology 29th Annual Conference*, pages 2655–2658, 2007.

[12] M. F. Chimeno and R. Pallàs-Areny. A comprehensive model for power line interference in biopotential measurements. *IEEE Transactions on Instrumentation and Measurement*, 49(3):535–540, June 2000.

[13] I. I. Christov and I. K. Daskalov. Filtering of electromyogram artifacts from the electrocardiogram. *Medical Engineering & Physics*, (21):731–736, 1999.

[14] R. Cobbold. *Transducers for Biomedical Measurements*. John Wiley & Sons, 1974. 486 p.

[15] J. C. Collias and E. E. Manuelidis. Histopathological changes produced by implanted electrodes in cat brains. *Journal of Neurosurgery*, 14(3):302–328, 1957.

[16] A. Cömert, M. Honkala, M. Puurtinen, and M. Perhonen. The suitability of silver yarn electrodes for mobile EKG monitoring. *14th Nordic-Baltic Conference on Biomedical Engineering and Medical Physics NBC 2008*, pages 198–201, June 2008.

[17] H. de Talhouet and J. G. Webster. The origin of skin-stretch-caused motion artifacts under electrodes. *Physiolgical Measurements*, 17:81–93, 1996.

[18] T. Degen and H. Jäckel. Continuous monitoring of electrode–skin impedance mismatch during bioelectric recordings. *IEEE Transactions on Biomedical Engineering*, 55(6):1711–1715, 2008.

[19] N. Donaldson and T. A. Perkins. Analysis of resonant coupled coils in the design of radio frequency transcutaneous links. *Journal of Medical and Biological Engineering and Computing*, 21:612–627, 1983.

[20] D. Dudenbostel, K.-L. Krieger, C. Candler, and R. Laur. A new passive CMOS telemetry chip to receive power and transmit data for a wide range of sensor applications. *Proceedings of TRANSDUCERS 97*, 2:995–998, 1997.

[21] A. M. Dymond, L. E. Kaechele, J. M. Jurist, and P. H. Crandall. Brain tissue reaction to some chronically implanted metals. *Journal of Neurosurgery*, 33(5):574–580, 1970.

[22] T. Eggers, C. Marschner, U. Marschner, B. Clasbrummel, R. Laur, and J. Binder. Advanced hybrid integrated low-power telemetric pressure monitoring system for biomedical applications. *Proceedings of IEEE Micro Electro Mechanical Systems (MEMS)*, pages 329–334, 2000.

[23] C. Enokawa, Y. Yonezawa, H. Maki, and M. Aritomo. A microcontroller-based implantable telemetry system for sympathetic nerve activity and ECG measurement. *Proceedings of the 19th International Conference of IEEE/EMBS*, pages 2232–2234, 1997.

[24] D. J. Farwell, N. Freemantle, and N. Sulke. The clinical impact of implantable loop recorders in patients with syncope. *European Heart Journal*, 27:351–356, 2006.

[25] T. Finnberg, A. Karilainen, and J. Müller. Mobile interrogation unit for passive SAW-sensors in long-term ECG-monitoring. *Proceedings of the 3rd European Medical and Biological Engineering Conference, Prague, Czech Rep., Nov 20-25*, 11(1), 2005.

[26] P. Fitch. Signal/noise ratio in the recording of human nerve-action potentials. *Medical and Biological Engineering*, pages 146–154, March 1973.

[27] W. Franks, I. Schenker, P. Schmutz, and A. Hierlemann. Impedance characterization and modeling of electrodes for biomedical applications. *IEEE Transactions on Biomedical Engineering*, 52(7):1295–1302, 2005.

[28] L. Geddes and L. Baker. *Principles of applied biomedical instrumentation*. Wiley, 1975. 616 p.

[29] L. A. Geddes. *Electrodes and the Measurements of Bioelectric Events*. Wiley, 1972. 364 p.

[30] L. A. Geddes. Historical evolution of circuit models for the electrode–electrolyte interface. *Annals of Biomedical Engineering*, 25:1–14, 1997.

[31] L. A. Geddes and L. E. Baker. The relationship between input impedance and electrode area in recording the ecg. *Medical and Biological Engineering*, 4:439–450, 1966.

[32] L. A. Geddes and R. Roeder. Criteria for the selection of materials for implanted electrodes. *Annals for Biomedical Engineering*, 31:879–890, 2003.

[33] C. Gondran, E. Siebert, S. Yacoub, and E. Novakow. Noise of surface bio-potential electrodes based on NASICON ceramic and Ag-AgCl. *Medical & Biological Engineering & Computing*, 34:460–466, 1996.

[34] D. H. Gordon. Triboelectric interference in the ECG. *IEEE Transactions on Biomedical Engineering*, BME-22(3):252–255, May 1975.

[35] S. Grimnes. Impedance measurement of individual surface electrodes. *Medical & Biological Engineering & Computing*, 21:750–755, 1983.

[36] F. W. Grover. *Inductance Calculations – Working Formulas and Tables*. D. van Nostrand Company, Inc., New York, 1946.

[37] C. J. Harland, T. D. Clark, and R. J. Prance. High resolution ambulatory electrocardiographic monitoring using wrist-mounted electric potential sensors. *Measurement Science and Technology*, 14:923–928, 2003.

[38] T. J. Harpster, S. Hauvespre, M. R. Dokmeci, and K. Najafi. A passive humidity monitoring system for in situ remote wireless testing of micropackages. *Journal of Microelectromechanical Systems*, 11(1):61–67, February 2002.

[39] T. J. Harpster, B. Stark, and K. Najafi. A passive wireless integrated humidity sensor. *Sensors and Actuators A*, 95:100–107, 2002.

[40] T. Hilbel, T. M. Helms, G. Mikus, H. A. Katus, and C. Zugck. Telemetry in the clinical setting. *Herzschrittmacherther Electrophysiol.*, 19(3):146–154, 2008.

[41] J. W. Horton and A. C. van Ravenswaay. Electrical impedance of the human body. *J. Franklin Inst.*, (220):557–572, 1935.

[42] J. C. Huhta and J. G. Webster. 60-Hz interference in electrocardiography. *IEEE Transactions*, BME-20:91–101, 1973.

[43] E. Huigen, A. Peper, and C. A. Grimbergen. Investigation into the origin of the noise of surface electrodes. *Journal of Medical and Biological Engineering and Computing*, 40:332–338, 2002.

[44] J. Hännikäinen, T. Vuorela, and J. Vanhala. Physiological measurements in smart clothing: A case study of total body water estimation with bioimpedance. *Transactions of the Institute of Measurement and Control*, 2007.

[45] IEEE/ANSI c95.1 – 2005. IEEE standard for safety levels with respect to human exposure to radio frequency electromagnetic fields, 3 kHz to 300 GHz. Standard, 2005.

[46] P. Irazoqui-Pastor, I. Mody, and J. W. Judy. In-vivo EEG recording using a wireless implantable neural transceiver. *IEEE Engineering in Medicine and Biology 25th Annual Conference*, 2003.

[47] R. S. Jutley, D. E. Shepherd, D. W. Hukins, and R. R. Jeffrey. Preliminary evaluation of the sternum screw: a novel method for improved sternal closure to prevent dehiscence. *Cardiovascular Surgery 2003 Feb;11(1):85-9*, 11(1):85–89, February 2003.

[48] A. Karilainen, T. Finnberg, T. Uelzen, K. Dembowski, and J. Müller. Mobile patient monitoring based on impedance-loaded SAW-sensors. *IEEE Transactions on Ultrasonics, Ferroelectrics and Frequency Control*, 51(11):1464–1469, November 2004.

[49] A. Karilainen, T. Finnberg, and J. Müller. Wireless passive sensor for measuring ECG and other biopotentials in impedance loaded SAW technology. *Proceedings of the 3rd European Medical and Biological Engineering Conference, Prague, Czech Rep., Nov 20-25*, 11(1), 2005.

[50] M. Kawashita, S. Tsuneyama, F. Miyaji, T. Kokubo, H. Kozuka, and K. Yamamoto. Antibacterial silver-containing silica glass prepared by sol-gel method. *Biomaterials*, 21:393–398, 2000.

[51] J. Kim and R.-S. Yahya. Electromagnetic interactions between biological tissues and implantable biotelemetry systems. *Microwave Symposium Digest, 2005 IEEE MTT-S International*, pages 1801–1804, 2005.

[52] W. Ko. *Biomedical Transducers*, chapter 1, pages 3–72. Academic Press Inc., 1988. In book Kline, Jacob (editor): Handbook of Biomedical Engineering, 733 p.

[53] W. H. Ko, P. Liang, Sheau, and C. D. F. Fung. Design of radio-frequency powered coils for implant measurements. *Journal of Medical and Biological Engineering and Computing*, 15(6):634–640, November 1977.

[54] G. T. A. Kovacs. *Enabling Technologies for Cultured Neural Networks*, chapter Introduction to the theory, design and modeling of thin-film microelectrodes for neural interfaces, pages 121–165. Academic, London, U.K., 1994.

[55] A. D. Krahn, G. J. Klein, C. Norris, and R. Yee. The etiology of syncope in patients with negative tilt table and electrophysiological testing. *Circulation*, 92(7):1819–1824, October 1995.

[56] K. Kramer, H.-P. Voss, J. A. Grimbergen, P. A. Mills, D. Huetteman, L. Zwiers, and B. Brockway. Telemetric monitoring of blood pressure in freely moving mice: a preliminary study. *Laboratory Animals*, 34:272–280, 2000.

[57] A. Kurs, A. Karalis, R. Moffatt, J. Joannopoulos, P. Fisher, and M. Soljačić. Wireless power transfer via strongly coupled magnetic resonances. *Science*, 317(83):83–86.

[58] J. Lario-García and R. Pallas-Arèny. Measurement of three independent components in impedance sensors using a single square wave. *Sensors and Actuators A*, (110): 164–170, 2004.

[59] J. Lario-García and R. Pallas-Arèny. Constant-phase element identification in conductivity sensors using a single square wave. *Sensors and Actuators A*, (132):122–128, 2006.

[60] J. Lario-García and R. Pallàs-Areny. Analysis of a three–component impedance using two sine waves. *IEEE Instrumentation and Measurement Technology Conference*, pages 1282–1284, 2003.

[61] R. Laukkanen and P. Virtanen. Heart rate monitors - state of the art. *Journal of Sports Sciences*, 16:S3–S7, 1998.

[62] G. Loriga, N. Taccini, D. De Rossi, and R. Paradiso. Textile sensing interfaces for cardiopulmonary signs monitoring. *IEEE Engineering in Medicine and Biology 27th Annual Conference*, September 2005.

[63] J. Malmivuo and R. Plonsey. *Bioelectromagnetism - Principles and Applications of Bioelectric and Biomagnetic Fields*. Oxford University Press, New York, 1995. 456 p.

[64] S. Malpas. A novel implantable blood pressure telemetry device; comparison between data sciences and telemetry research systems. *Journal of Pharmacological and Toxicological Methods*, 60(2):235, 2009.

[65] E. McAdams and J. Jossinet. Electrode–electrolyte interface impedance: The limit current of linearity. *Annual International Conference of the IEEE Engineering in Medicine and Biology Society*, 13(4):1728–1729, 1991.

[66] E. T. McAdams and J. Jossinet. Tissue impedance: a historical overview. *Physiological Measurements*, 16:A1–A13, 1995.

[67] E. T. McAdams, J. Jossinet, A. Lackermeier, and F. Risacher. Factors affecting electrode-gel-skin interface impedance in electrical impedance tomography. *Medical & Biological Engineering & Computing*, 34:397–408, 1996.

[68] E. T. McAdams, J. Jossinet, R. Subramanian, and R. G. E. McCauley. Characterization of gold electrodes in phosphate buffered saline solution by impedance and noise measurements for biological applications. *Proceedings of the 28th IEEE EMBS Annual International Conference*, pages 4594–4597, 2006.

[69] G. Medrano, L. Beckmann, N. Zimmermann, T. Grundmann, T. Gries, and S. Leonhardt. Bioimpedance spectroscopy with textile electrodes for a continuous monitoring application. *4th International Workshop on Wearable and Implantable Body Sensor Networks (BSN 2007)*, 13:23–28, 2007.

[70] G. Medrano, A. Ubl, N. Zimmermann, T. Gries, and S. Leonhardt. Skin electrode impedance of textile electrodes for bioimpedance spectroscopy. *Proceedings of 13th International Conference on Electrical Bioimpedance and the 8th Conference on Electrical Impedance Tomography*, 17:260–263, 2007.

[71] G. Medrano, L. Beckmann, M. Gube, R. Kasim, S. Kim, T. Kraus, and S. Leonhardt. Continuous hand-to-foot and segmental bioimpedance spectroscopy measurements within a period of five days. *Proceedings of World Congress on Medical Physics and Biomedical Engineering*, pages 122–125, 2009.

[72] Medtronic Inc. Reveal® DX insertable cardiac monitor (ICM). Website. URL http://www.medtronic.com/physician/reveal/index.html. Accessed 20.10.2009.

[73] A. C. Metting van Rijn, A. Peper, and C. A. Grimbergen. High-quality recording of bioelectric events - part 1. *Medical & Biological Engineering & Computing*, 28(5): 389–397, 1990.

[74] A. C. Metting van Rijn, A. P. Kuiper, T. E. Dankers, and C. A. Grimbergen. Low-cost active electrode improves the resolution in biopotential recordings. *18th Annual International Conference of the IEEE Engineering in Medicine and Biology Society*, pages 101–102, 1996.

[75] Y. Ming. *A Multi-Channel Wireless Implantable Neural Recording System*. PhD thesis, North Carolina State University, 2009.

[76] C. D. Motchenbacher and F. C. Fitchen. *Low-Noise Electronic Design*. John Wiley & Sons, 1973. 358 p.

[77] F. Moussy and D. J. Harrison. Prevention of the rapid degradation of subcutaneously implanted Ag/AgCl reference electrodes using polymer coatings. *Analytical Chemistry*, 66:674–679, 1994.

[78] J. Mühlsteff and O. Such. Dry electrodes for monitoring of vital signs in functional textiles. *IEEE Engineering in Medicine and Biology 26th Annual Conference*, pages 2212–2215, 2004.

[79] J. Mühlsteff, O. Such, R. Schmidt, M. Perkuhn, H. Reiter, J. Lauter, J. Thijs, G. Müsch, and M. Harris. Wearable approach for continuous ECG – and activity patient-monitoring. *IEEE Engineering in Medicine and Biology 26th Annual Conference*, pages 2184–2187, September 1-5 2004.

[80] J. H. Nagel. *The Biomedical Engineering Handbook*, chapter Biopotential Amplifiers. CRC Press LLC, 2nd edition, 2000.

[81] N. Najafi and A. Ludomirsky. Initial animal studies of a wireless, batteryless, MEMS implant for cardiovascular applications. *Biomedical Microdevices*, 6(1):61–65, 2004.

[82] S. N. Nihtianov, G. P. Sheterev, B. Iliev, and G. C. M. Meijer. A novel technique to measure two independent components of impedance sensors with a simple relaxation

oscillator. *Instrumentation and Measurement Technology Conference, 2000. IMTC 2000*, pages 674–678, 2000.

[83] S. Nishimura, Y. Tomita, and T. Horiuchi. Clinical application of an active electrode using an operational amplifier. *IEEE Transactions on Biomedical Engineering*, 39(10): 1096–1099, 1992.

[84] N. Noury, A. Dittmar, C. Corroy, R. Baghai, J. L. Weber, D. Blanc, F. Klefstat, A. Blinovska, S. Vaysse, and CometB. A smart cloth for ambulatory telemonitoring of physiological parameters and activity: The VTAMN project. *IEEE Engineering in Medicine and Biology 26th Annual Conference*, pages 155–160, 2004.

[85] S. Oh, J. Lee, K. Jeong, and L. Lee. Minimization of electrode polarization effect by nanogap electrodes for biosensor applications. *IEEE The Sixteenth Annual International Conference on Micro Electro Mechanical Systems, 2003. MEMS-03 Kyoto.*, pages 52–55, 2003.

[86] N. B. Olivier, E. Nolan, B. Olivier, and D. Singer. A comparative study of surface telemetry and implantable telemetry. *Journal of Pharmacological and Toxicological Methods*, 56(2):e57, 2007.

[87] J. Ottenbacher, S. Römer, C. Kunze, U. Großmann, and W. Stork. Integration of a bluetooth based ECG system into clothing. *Eighth International Symposium on Wearable Computers (ISWC'04)*, 2004.

[88] R. Paradiso. Knitted textile for the monitoring of vital signals. United Stated Patent Application Publication number WO2005053532, April 2007.

[89] R. Paradiso and D. De Rossi. Advances in textile technologies for unobtrusive monitoring of vital parameters and movements. *Proceedings of the 28th IEEE EMBS Annual International Conference*, pages 392–395, 2006.

[90] R. Paradiso, G. Loriga, and N. Taccini. A wearable health care system based on knitted integrated sensors. *IEEE Transactions on Information Technology in Biomedicine*, 9 (3):337–344, September 2005.

[91] R. Paradiso, G. Loriga, N. Taccini, A. Gemignani, and B. Ghelarducci. WEALTHY – a wearable healthcare system: new frontier on e-textile. *Journal of Telecommunications and Information Technology*, (4):105–113, 2005.

[92] R. Parsons. *The Encyclopedia of Electrochemistry*. Reinhold, New York, 1964. 1206 p.

[93] T. Pawar, N. S. Anantakrishnan, and S. Chaudhuri. Transition detection in body movement activities for wearable ECG. *IEEE Transactions on Biomedical Engineering*, 54 (6):1149–1152, June 2007.

[94] J. A. Potkay. Long term, implantable blood pressure monitoring systems. *Biomedical Microdevices*, 10:379–392, 2008.

[95] M. Puurtinen, S. Komulainen, P. Kauppinen, and J. Malmivuo. Measurement of noise and impedance of dry and wet textile electrodes, and textile electrodes with hydrogel. *Proceedings of the 28th IEEE EMBS Annual International Conference*, pages 6012–6015, August 2006.

[96] M. Qu, Y. Zhang, J. G. Webster, and W. J. Tompkins. Motion artifact from spot and band electrodes during impedance cardiography. *IEEE Transactions on biomedical engineering*, BME–33(11):1029–1036, November 1986.

[97] J. E. Randles. Kinetics of rapid electrode reactions. *Discussions of Faraday Society 1*, 11:11–19, 1947.

[98] R. W. Revie, editor. *Uhlig's Corrosion Handbook*. John Wiley & Sons, Inc., 2nd edition, 2000. 1340 p.

[99] F. R. Robinson and M. T. Johnson. Histopathological studies of tissue reactions to various metals implanted in cat brains. Aeronautical Systems Div Wright-Patterson AFB Ohio Aerospace Medical Div, October 1961.

[100] G. Rondelli, P. Torricelli, M. Fini, and R. Giardino. In vitro corrosion study by EIS of a nickel-free stainless steel for orthopaedic applications. *Biomaterials*, (26):739–744, 2004.

[101] J. Rosell, J. Colominas, P. Riu, R. Pallàs-Areny, and J. G. Webster. Skin impedance from 1 Hz to 1 MHz. *IEEE Transactions on Biomedical Engineering*, 35(8):649–651, August 1988.

[102] E. M. Schmidt, J. S. McIntosh, and M. J. Bak. Long-term implants of parylene-c coated microelectrodes. *Medical and Biological Engineering and Computing*, 26:96–101, 1988.

[103] H. P. Schwan. Linear and nonlinear electrode polarization and biological materials. *Annals of Biomedical Engineering*, 20:269–288, 1992.

[104] H. P. Schwan. Electrode polarization impedance and measurements in biological materials. *Annals of the New York Academy of Sciences*, 148:191–209, 1968.

[105] A. S. Sedra and K. C. Smith. *Microelectronic Circuits*. Oxford University Press, 4th edition, 1998. 1237 p.

[106] V.-P. Seppä, J. Väisänen, P. Kauppinen, J. Malmivuo, and J. Hyttinen. Measuring respirational parameters with wearable bioimpedance device. *Proceedings of 13th International Conference on Electrical Bioimpedance and the 8th Conference on Electrical Impedance Tomography*, 17:663–666, 2007.

[107] V.-P. Seppä, O. Lahtinen, J. Väisänen, and J. Hyttinen. Assessment of breathing parameters during running with a wearable bioimpedance device. *4th European Conference of the International Federation for Medical and Biological Engineering ECIFMBE 2008*, 22:1088–1091, November 2008.

[108] V.-P. Seppä, J. Viik, A. Naveed, J. Väisänen, and J. Hyttinen. Signal waveform agreement between spirometer and impedance pneumography of six chest band electrode configurations. *Proceedings of World Congress on Medical Physics and Biomedical Engineering*, pages 689–692, 2009.

[109] M. Spinelli, N. H. Martínez, and M. A. Mayosky. A transconductance driven-right-leg circuit. *IEEE Transactions on Biomedical Engineering*, 46(12):1466–1470, December 1999.

[110] S. S. Stensaas and L. J. Stensaad. Histopathological evaluation of materials implanted in the cerebral cortex. *Acta Neuropathologica*, 41:145–155, 1978.

[111] Y.-T. Sul, C. B. Johansson, Y. Jeong, and T. Albrektsson. The electrochemical oxide growth behaviour on titanium in acid and alkaline electrolytes. *Medical Engineering & Physics*, 23(5):329–346, 2001.

[112] S. M. Sunderarajan. *Design, modeling and optimization of on-chip inductor and transformer circuits*. PhD thesis, Stanford University, 1999.

[113] H. Suzuki, T. Hirakawa, S. Sasaki, and I. Karube. An integrated three-electrode system with a micromachined liquid-junction Ag/AgCl reference electrode. *Analytica Chimica Acta*, 387:103–112, 1999.

[114] L. Sörnmo and P. Laguna. *Bioelectrical Signal Processing in Cardiac and Neurological Applications*. Elsevier Inc., London, UK, 2005. 688 p.

[115] K. Takahata, A. DeHennis, K. D. Wise, and Y. B. Gianchandani. Stentenna: A micromachined antenna stent for wireless monitoring of implantable microsensors. *IEEE Engineering in Medicine and Biology 25th Annual Conference*, pages 3360–3363, 2003.

[116] P. Talonen. *A More Natural Approach to Nerve Stimulation in Electrophrenic Respiration*. PhD thesis, Tampere University of Technology, 1990.

[117] Z. Tang, B. Smith, J. H. Schild, and P. H. Peckham. Data transmission from an implantable biotelemeter by load-shift keying using circuit configuration modulator. *IEEE Transactions on Biomedical Engineering*, 42(5):524–528, 1995.

[118] Texas Instruments. INA333 micro-power (50μA), zerø-drift, rail-to-rail out instrumentation amplifier. Data Sheet, 2008.

[119] N. V. Thakor and J. G. Webster. Ground-free ECG recording with two electrodes. *IEEE Transactions on Biomedical Engineering*, BME-27(12):699–704, December 1980.

[120] N. V. Thakor and J. G. Webster. The origin of skin potential and its variations. *Proceedings of the 31st Annual Conference on Engineering in Biology and Medicine*, 20, 1978. 212 p.

[121] B. C. Towe. Passive backscatter biotelemetry for neural interfacing. *IEEE EMBS Conference on Neural Engineering*, pages 144–147, May 2007.

[122] P. Valdastri, S. Rossi, A. Menciassi, V. Lionetti, F. Bernini, F. A. Recchia, and P. Dario. An implantable ZigBee ready telemetric platform for in vivo monitoring of physiological parameters. *Sensors and Actuators A*, (142):369–378, 2008.

[123] M. E. Valentinuzzi, J.-P. Morucci, and C. J. Felice. *Critical Reviews in Biomedical Engineering*, volume 24, chapter Bioelectrical Impedance Techniques in Medicine; Part II: Monitoring of Physiological Events by Impedance, pages 353–466. Begell House Inc., 1996.

[124] K. van Kuyck, M. Welkenhuysen, L. Arckens, R. Sciot, and B. Nuttin. Histological alterations induced by electrode implantation and electrical stimulation in the human brain: A review. *Neuromodulation: Technology at the Neural Interface*, 10(3):244–261, 2007.

[125] K. Van Schuylenbergh and R. Puers. Self-tuning inductive powering for implantable telemetric monitoring systems. *Sensors and Actuators A*, 52:1–7, 1996.

[126] K. J. Vetter. *Elektrochemische Kinetik*. Springer-Verlag, 1961. 698 p.

[127] T. Vuorela, V.-P. Seppä, J. Vanhala, and J. Hyttinen. Two portable long-term measurement devices for ECG and bioimpedance. *Proceedings of the second International Conference on Pervasive Computing Technologies for Healthcare 2008*, pages 169–172, January 2008.

[128] T. Vuorela, V.-P. Seppä, J. Vanhala, and J. Hyttinen. Design and implementation of a portable long-term physiological signal recorder. *Transactions on Information Technology in BioMedicine*, 2009. Submitted June 30th 2009.

[129] J. Väisänen, J. Hyttinen, M. Puurtinen, P. Kauppinen, and J. Malmivuo. Prediction of implantable ECG lead systems by using thorax models. *IEEE Engineering in Medicine and Biology 26th Annual Conference*, pages 809–812, September 1-5 2004.

[130] D. E. Watson and D. M. Yee. Behaviour of Ag/AgCl electrodes in solutions containing both Cl^- and I^-. *Electrochimica Acta*, 14:1143–1153, 1969.

[131] B. B. Winter and J. G. Webster. Driven-right-leg circuit design. *IEEE Transactions on Biomedical Engineering*, BME-30:62–66, 1983.

[132] D. E. Wood, D. J. Ewins, and W. Balachandran. Comparative analysis of power-line interference between two-or three-electrode biopotential amplifiers. *Medical & Biological Engineering & Computing*, 33:63–68, 1995.

[133] C. Yue, Patric and S. Wong, Simon. Physical modeling of spiral inductors on silicon. *IEEE Transactions on Electron Devices*, 47(3):560–568, March 2000.

[134] F. Zhang, Z. Zheng, Y. Chen, X. Liu, A. Chen, and Z. Jiang. *In vivo* investigation of blood compatibility of titanium oxide films. *Journal of Biomedical Material Research*, 42:128–133, 1998.

[135] C. M. Zierhofer and E. S. Hochmair. Geometric approach for coupling enhancement of magnetically coupled coils. *IEEE Transactions on biomedical engineering*, 43(7): 708–714, July 1996.

[136] C. M. Zierhofer and E. S. Hochmair. Coil design for improved power transfer efficiency in inductive links. *Proceedings of 18th Annual International Conference of the IEEE Engineering in Medicine and Biology Society*, pages 1538–1539, 1996.

[137] S. Ödman. Changes in skin potentials induced by skin compression. *Medical & Biological Engineering & Computing*, 27:390–393, 1989.

PUBLICATION P1

Riistama, J. and Lekkala, J. "Electrode-electrolyte Interface Properties in Implantation Conditions," in *Proceedings of the 28th Annual International Conference of the IEEE Engineering in Medicine and Biology Society – EMBC. Engineering Revolution in Biomedicine*, New York City, New York, USA. p. 6021–6024. 30 August–3 September, 2006.

Publication to be provided on request, email to jarno.riistama@tut.fi.

PUBLICATION P2

Riistama, J. and Lekkala, J. “Electrochemical noise properties of different electrode materials in different electrolytes”, in Leonhardt, S., Falck, T. & Mähönen, P. (Eds.). *IFMBE Proceedings. Volume 13. 4th International Workshop on Wearable and Implantable Body Sensor Networks (BSN 2007)*, RWTH Aachen University, Germany, pp. 149–154, March 26–28, 2007.

Publication to be provided on request, email to jarno.riistama@tut.fi.

PUBLICATION P3

Riistama, J., Väisänen, J., Heinisuo, S., Lekkala, J. and Kaihilahti, J. "Evaluation of an implantable ECG monitoring device *in vitro* and *in vivo*", in *Proceedings of the 29th Annual International Conference of the IEEE EMBS Engineering in Medicine and Biology Society in conjunction with the Biennial Conference of the French Society of Biological and Medical Engineering (SFGBM)*, Lyon, France. pp. 5703–5706, August 23–26, 2007.

Publication to be provided on request, email to jarno.riistama@tut.fi.

PUBLICATION P4

Riistama, J., Väisänen, J., Heinisuo, S., Harjunpää, H., Arra, S., Kokko, K., Mäntylä, M., Kaihilahti, J., Heino, P., Kellomäki, M., Vainio, O., Vanhala, J., Lekkala, J. and Hyttinen, J. "Wireless and inductively powered implant for measuring electrocardiogram", Medical & Biological Engineering & Computing **45**:1163–1174, 2007.

Publication to be provided on request, email to jarno.riistama@tut.fi.

PUBLICATION P5

Riistama, J., Aittokallio, E., Verho, J. and Lekkala, J. “Totally passive wireless biopotential measurement sensor by utilizing inductively coupled resonance circuits”, Sensors and Actuators A – Physical **157**(2):313–321, 2010.

Publication to be provided on request, email to jarno.riistama@tut.fi.

PUBLICATION P6

Riistama, J., Röthlingshöfer, L., Leonhardt, S. and Lekkala, J. “Noise and interface impedance of textile electrodes on simulated skin interface”, Medical & Biological Engineering & Computing, 2010, *submitted*.

Publication to be provided on request, email to jarno.riistama@tut.fi.